FRONTIERS OF PHYSICS

TOPICAL REVIEW
Volume 18 / Issue 2 / 21307 / 2023

Quantum transport in topological semimetals under magnetic fields (III)

Lei Shi[1,2], Hai-Zhou Lu[1,2,†]

1 Shenzhen Institute for Quantum Science and Engineering and Department of Physics, Southern University of Science and Technology, Shenzhen 518055, China
2 Shenzhen Key Laboratory of Quantum Science and Engineering, Shenzhen 518055, China
Corresponding author. E-mail: †luhz@sustc.edu.cn
Received January 13, 2023; accepted March 15, 2023

ABSTRACT

We review our most recent research on quantum transport, organizing the review according to the intensity of the magnetic field and focus mostly on topological semimetals and topological insulators. We first describe the phenomenon of quantum transport when a magnetic field is not present. We introduce the nonlinear Hall effect and its theoretical descriptions. Then, we discuss Coulomb instabilities in 3D higher-order topological insulators. Next, we pay close attention to the surface states and find a function to identify the axion insulator in the antiferromagnetic topological insulator $MnBi_2Te_4$. Under weak magnetic fields, we focus on the decaying Majorana oscillations which has the correlation with spin–orbit coupling. In the section on strong magnetic fields, we study the helical edge states and the one-sided hinge states of the Fermi-arc mechanism, which are relevant to the quantum Hall effect. Under extremely large magnetic fields, we derive a theoretical explanation of the negative magnetoresistance without a chiral anomaly. Then, we show how magnetic responses can be used to detect relativistic quasiparticles. Additionally, we introduce the 3D quantum Hall effect's charge-density wave mechanism and compare it with the theory of 3D transitions between metal and insulator driven by magnetic fields.

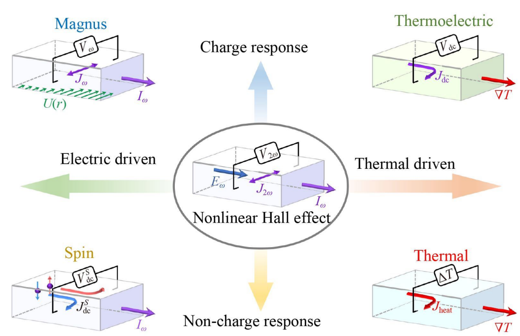

Keywords topological semimetal, topological insulator, axion insulator, nonlinear Hall effect (NHE), quantum oscillation, quantum Hall effect (QHE), charge density wave (CDW)

Contents

*Special Topic: Embracing the Quantum Era: Celebrating the 5th Anniversary of Shenzhen Institute for Quantum Science and Engineering (Eds.: Dapeng Yu, Dawei Lu & Zhimin Liao).

Higher Education Press

https://doi.org/10.1007/s11467-023-1259-5

1 Introduction

Quantum transport, especially in topological matter, is a fascinating and increasingly important field of condensed matter physics. We previously reviewed our research on quantum transport phenomena in Refs. [1–3]. The studies discussed in those reviews concerned such topics as weak localization (and weak antilocalization) [4, 5], negative magnetoresistance [6, 7], quantum oscillations in nodal-line semimetals [8] and Weyl semimetals [9], magneto-transport in the quantum limit [10, 11], the 3D quantum Hall effect [12], vanishing backscattering [13] and Weyl-node annihilation [14].

In this paper, we introduce latest works of ours which were not addressed in Refs. [1, 2]. In Section 2, we will introduce some models used in this review. In Section 3, we summarize the nonlinear Hall effect from two theoretical perspectives: the semiclassical theory and the quantum theory described by Feynman diagrams [15–19]. In Section 4, we survey Coulomb instabilities in higher-order topological insulators (TIs) [20]. In Section 5, we present an analytical solution of anti-ferromagnetic TI $MnBi_2Te_4$ for the surface states [21]. In Section 6, we use a new method to identify the axion insulator which called nonlocal surface transport [22]. In Section 7, we reveal the decaying Majorana oscillations which may induced by the spin–orbit coupling's steplike distribution [23]. In Section 8, we propose that there are highly tunable one-sided hinge states via the direction of field and Fermi energy in Cd_3As_2-like Dirac semimetals [24]. In Section 9, we analyze how the growth direction, Fermi energy, and thickness affect the QHE in topological semimetals [25]. In Section 10, we explain the negative magnetoresistance of Kramers Weyl semimetals in the quantum limit [26]. In Section 11, we propose a method for using magnetic responses to detect relativistic quasi-particles [27]. In Section 12, we introduce a theory of the 3D QHE for the CDW mechanism, which captures the key characteristics observed in experiments [28]. In Section 13, we present a scaling theory for the transitions between metal and insulator in a three-dimensional system's quantum limit [29].

2 Effective models

In this section, we will introduce some models mentioned in this review.

2.1 Weyl semimetals

In general, we use a two-node Hamiltonian [30–33] model to describe the Weyl semimetal,

$$H = A(k_x\sigma_x + k_y\sigma_y) + M(k_w^2 - \boldsymbol{k}^2)\sigma_z, \tag{2.1}$$

where $\boldsymbol{k} = (k_x, k_y, k_z)$ is the wave vector, σ_i $(i = x, y, z)$ are the Pauli matrices, and M, A, and k_w are the model parameters. The eigen energies are $E_\pm^{\boldsymbol{k}} = \pm[M^2(k_w^2 - \boldsymbol{k}^2)^2 + A^2(k_x^2 + k_y^2)]^{1/2}$, with "−" for the valence band and "+" for the conduction band. The two Weyl nodes are at $(0, 0, \pm k_w)$. This model has been demonstrated to capture the whole properties of topological semimetals [32]. This ability is attributable to the σ_z term in the model [34].

2.2 Dirac semimetals

The Hamiltonian for a Dirac semimetal can be expressed as [35–37]

$$H = \varepsilon_0(\boldsymbol{k}) + \begin{pmatrix} M(\boldsymbol{k}) & Ak_+ & 0 & 0 \\ Ak_- & -M(\boldsymbol{k}) & 0 & 0 \\ 0 & 0 & M(\boldsymbol{k}) & -Ak_- \\ 0 & 0 & -Ak_+ & -M(\boldsymbol{k}) \end{pmatrix}, \tag{2.2}$$

where $k_\pm = k_x \pm \mathrm{i}k_y$, $\varepsilon_0(\boldsymbol{k}) = C_0 + C_1k_z^2 + C_2(k_x^2 + k_y^2)$, and $M(\boldsymbol{k}) = M_0 + M_1k_z^2 + M_2(k_x^2 + k_y^2)$. In the model presented in Section 8, the [100], [010], and [001] crystallographic directions, respectively, define the x, y, and z axes. At $\boldsymbol{k} = (0, 0, \pm k_\mathrm{w})$ the model has two pairs of Weyl nodes. The energies $E_\mathrm{w} = C_0 - C_1M_0/M_1$ and $k_\mathrm{w} = \sqrt{|M_0/M_1|}$.

2.3 Topological insulators

In Section 5, the 3D TI is expressed as

$$\mathcal{H}(\boldsymbol{k}) = \epsilon_0(\boldsymbol{k}) + \begin{pmatrix} M(\boldsymbol{k}) & A_1k_z & 0 & A_2k_- \\ A_1k_z & -M(\boldsymbol{k}) & A_2k_- & 0 \\ 0 & A_2k_+ & M(\boldsymbol{k}) & -A_1k_z \\ A_2k_+ & 0 & -A_1k_z & -M(\boldsymbol{k}) \end{pmatrix} + H_X, \tag{2.3}$$

where $\epsilon_0(\boldsymbol{k}) = C_0 + D_1 k_z^2 + D_2(k_x^2 + k_y^2)$, $k_\pm = k_x \pm \mathrm{i}k_y$, and $M(\boldsymbol{k}) = M_0 - B_1 k_z^2 - B_2(k_x^2 + k_y^2)$. Here, M_0, A_i, B_i, C_0 and D_i are model parameters. H_X is the exchange field that we characterize using the sinusoidal function for simplicity. The basis of the Hamiltonian is $\{|P1_z^+, \uparrow\rangle, |P2_z^-, \uparrow\rangle, |P1_z^+, \downarrow\rangle, |P2_z^-, \downarrow\rangle\}$.

In Section 4, the 3D second-order TI's four-band Hamiltonian is expressed as

$$\mathcal{H}_0(\check{k}) = \Big[M + \sum_i t_i \cos(ak_i)\Big]\tau_z\sigma_0 + \sum_i \Delta_i \sin(ak_i) \times \tau_x\sigma_i + \Delta_2[\cos(ak_x) - \cos(ak_y)]\tau_y\sigma_0, \tag{2.4}$$

where σ_i and τ_i are the Pauli matrices, a is the lattice constant, and t_i, M, Δ_2, and Δ_i are the hopping parameters. We take $t_x = t_y = t_\perp$ and $\Delta_x = \Delta_y = \Delta_\perp$. This model breaks the time-reversal symmetry $\mathcal{T}$ and four-fold rotation symmetry C_{4z} but respects their combination $C_{4z}\mathcal{T}$ if $\Delta_2 \neq 0$.

2.4 Kramers Weyl semimetals

The effective model suggested in Ref. [38] can adequately explain a Kramers Weyl cone,

$$\mathcal{H} = u(k_x^2 + k_y^2 + k_z^2) + v(k_x\sigma_x + k_y\sigma_y + k_z\sigma_z). \tag{2.5}$$

In the original model, the model parameters v and u have anisotropy which has been suppressed. This model's energy spectrum is

$$E_\pm(\boldsymbol{k}) = u(k_x^2 + k_y^2 + k_z^2) \pm v\sqrt{k_x^2 + k_y^2 + k_z^2} \tag{2.6}$$

in the plane $k_x = k_y = 0$.

3 Zero field: Nonlinear Hall effects

In condensed matter physics, the study of Hall effects has a long history. Hall effects hold a significant position in the field and continue to inspire new discoveries [39–43]. The hallmark of these effects is a transverse voltage that is triggered by longitudinal currents. In general, the Hall effect occurs when time-reversal symmetry is broken, which is often accomplished by providing a magnetic field [44].

The nonlinear Hall effect (NHE) [18, 19, 45–50] is a fascinating addition to the family of Hall effects. It is nonlinear in the sense that the Hall voltage is nonlinearly reliant on the longitudinal current; for example, there may be a quadratic relationship between the response voltage and driving current. The traditional Hall voltage, in contrast, is linearly related to the longitudinal current. In addition, only breaking inversion symmetry can generate nonlinear Hall effect, unlike the traditional Hall effect, which requires breaking time-reversal symmetry.

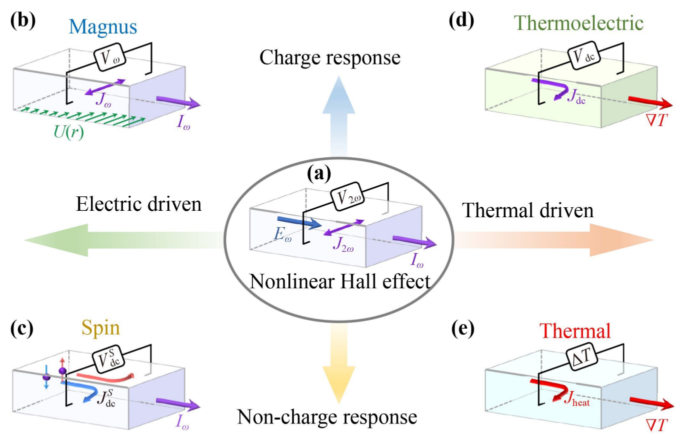

Fig. 1 This picture shows the method of Hall effect measurement. The lock-in technique is used to amplify the nonlinear Hall signal. An input ultralow-frequency current I_ω produces a response transverse voltage $V_{2\omega}$. The NHE can be generalized by substituting another response stimulus for the electric driving field [51–58]. Reproduced from Ref. [16].

This section introduces the NHE and presents the most recent advances in this area. We start by discussing the measurement of the NHE, then proceed to presenting the semiclassical Boltzmann theory, including the disorder-induced contributions to the effect, symmetry analysis, and other important aspects. Finally, we discuss the NHE from the quantum theory perspective and present the relevant Feynman diagrams.

3.1 Experimental measurements

A Hall bar is typically used in experiments to gauge the Hall effect (Fig. 1), in combination with the lock-in technique to muffle noise. Across the device, a transverse voltage with the same frequency, V_ω, is measured while a low-frequency alternating current, I_ω, is passed longitudinally over the Hall bar. The NHE is measured similarly, except that either double frequency $V_{2\omega}$ or zero frequency V_0 are used to determine the Hall voltage.

The NHE has been theoretically predicted in 2D transition metal dichalcogenides [19, 45, 46, 48, 49], 3D Weyl semimetals [45, 47, 50], the surfaces of crystalline TIs [45], and the 2D transition metal dichalcogenides [19, 45, 46, 48, 49]. Low-symmetry systems exhibiting this nonlinear quantum transport phenomenon are highly desired, and symmetry-breaking engineering has been used to realize such systems [16].

The NHE was early seen in 2D layers of WTe_2 [18, 59], a material with time-reversal symmetry. Utilizing encapsulated bilayer WTe_2 [Fig. 2(a)], one study observed a double frequency transverse current induced by a longitudinal a.c. excitation current with frequency ω of 10–1000 Hz at T = 10–100. The measurements in that study revealed clear quadratic I–V relationships [Fig.

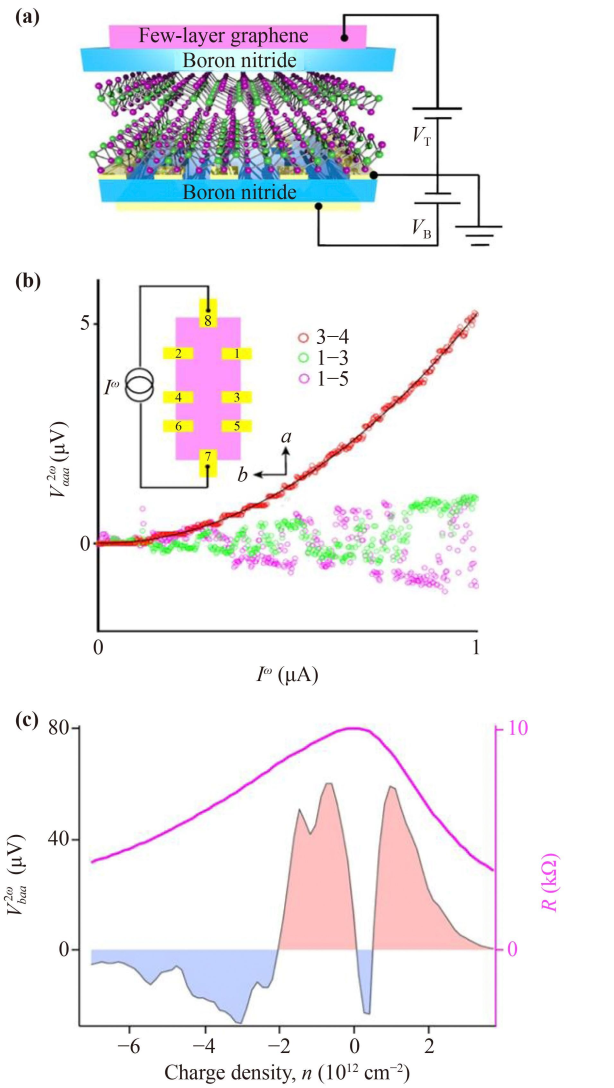

Fig. 2 **(a)** A bilayer WTe_2 device with dual-gated. **(b)** The different I–V curves due to the measurement from different electrodes. **(c)** The black line shows the Hall voltage $V^{2\omega}_{baa}$, the red line depicts resistance R. Abscissa axis is charge density. The blue (red) area marks the negative (positive) voltage $V^{2\omega}_{baa}$. Reproduced from Ref. [18].

2(b)]. Furthermore, the carrier density and electrical displacement field that is out of plane could be used to tune the sign of the NHE [Fig. 2(c)] using the bottom and top gate voltages. This experiment confirmed the existence of the NHE.

3.2 Semiclassical theory

Both extrinsic and intrinsic contributions lead to the NHE. The intrinsic part is determined by the quantum geometry of the band structure, while disorder contributes to the extrinsic part.

The Berry curvature [60] can describe the NHE, given that the only factor that influences the intrinsic contribution to conductivity is the band structure of a flawless crystal. For an ideal lattice, the Kubo formula can be used to calculate the following result [43]:

$$\sigma^{in}_{ij} = -\frac{e^2}{\hbar}\varepsilon_{ijl}\int \frac{\mathrm{d}^n}{(2\pi)^n}\Omega_c f_0. \tag{3.1}$$

Eq. (3.1) describes the relationship between the Berry curvature Ω and linear Hall conductivity. This integral equation has been used to calculate the intrinsic part of the anomalous Hall effect (AHE) [43, 61, 62].

In contrast, the nonlinear conductivity tensor χ_{abc} is [45, 46]

$$\chi_{abc} = \frac{\epsilon^{acd} D_{bd} e^3 \tau}{2\hbar^2(1+\mathrm{i}\omega\tau)}, \tag{3.2}$$

where τ is the relaxation time. The Berry curvature dipole is defined as

$$D_{bd} = \sum_n \int \frac{\mathrm{d}^d k}{(2\pi)^d}\left(\partial_{k_b}\Omega^d_k\right) f_0. \tag{3.3}$$

The disorder-induced extrinsic part, like the anomalous Hall effect, has two mechanisms: side-jump and skew-scattering contributions. Disorder-induced transverse displacement δr is the cause of the side-jump mechanism. When approaching and departing from an impurity, a coordinate shift δr is produced, which causes an energy shift which changes the rate of scattering. After numerous scatterings, these displacements are accumulated and give rise to an effective transverse velocity.

As the name implies, the skew-scattering mechanism involves transverse scattering that is asymmetric. We can expand the rate of scattering in the disorder strength up to the fourth order as follows:

$$\omega_{ll'} = \omega^{(2)}_{ll'} + \omega^{(3)}_{ll'} + \omega^{(4)}_{ll'}, \tag{3.4}$$

where $\omega^{(2)}_{ll'}$ is the pure symmetric term and is the leading symmetric contribution. $\omega^{(3)}_{ll'}$ and $\omega^{(4)}_{ll'}$ are the antisymmetric parts and dominate the skew-scattering contribution. The first contains the non-Gaussian disorder distribution, and the second contains the Gaussian disorder distribution.

3.3 Quantum theory

The NHE is a quantum transport phenomenon related to the Berry curvature. This section diagrammatically introduces the quantum theory of the NHE under disorder effects.

Different with the linear-response theory's bubble diagrams, we can use triangle and two-photon diagrams to describe the quadratic responses, which represent two inputs and one output, respectively. Quantum theory identifies 69 Feynman diagrams and, like semiclassical

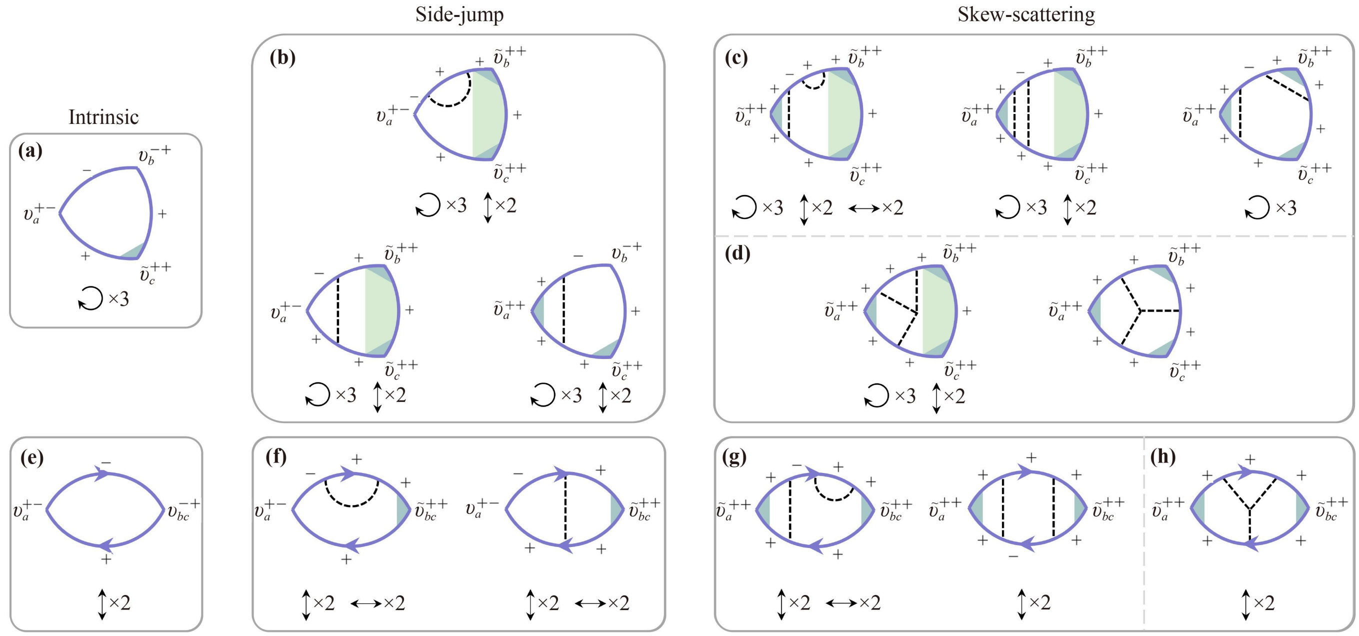

Fig. 3 **(a)** and **(e)** are diagrams of the intrinsic contribution. **(b)** and **(f)** are diagrams of the side-jump contribution. **(c)** and **(g)** are diagrams of intrinsic skew-scattering. **(d)** and **(h)** are diagrams of extrinsic skew-scattering. More diagrams can be found in the supplementary section of Ref. [15]. Reproduced from Ref. [15].

theory, takes into account skew-scattering, side-jump, and the intrinsic contributions. Figure 3 shows the resulting diagrams with the non-crossed approximation. The crucial disorder effects are taken into consideration in 64 of these diagrams and give rise to dramatic differences from nonlinear optics. We can use these diagrams for a general two-band model to calculate a disordered 2D tilted Dirac model's nonlinear Hall conductivity. These general formulas can be used in first-principles calculations.

The quadratic conductivity in the d.c. limit is calculated by $\chi_{abc} = \chi^{I}_{abc} + \chi^{II}_{abc} + \chi^{III}_{abc}$, where

$$\chi^{I}_{abc} = -\frac{e^3\hbar^2}{4\pi}\int[\mathrm{d}k]\int_{-\infty}^{\infty}\mathrm{d}\varepsilon\frac{\partial f(\varepsilon)}{\partial\varepsilon}\mathrm{Im}\Big\{\mathrm{Tr}\Big[\hat{v}_a\frac{\partial\hat{G}^R(\varepsilon)}{\partial\varepsilon}\hat{v}_b\hat{G}^R(\varepsilon)\hat{v}_c\hat{G}^A(\varepsilon)\Big]\Big\} + b\leftrightarrow c, \tag{3.5}$$

$$\chi^{II}_{abc} = -\frac{e^3\hbar^2}{8\pi}\int[\mathrm{d}k]\int_{-\infty}^{\infty}\mathrm{d}\varepsilon\frac{\partial f(\varepsilon)}{\partial\varepsilon}\mathrm{Im}\Big\{\mathrm{Tr}\Big[\hat{v}_a\frac{\partial\hat{G}^R(\varepsilon)}{\partial\varepsilon}\hat{v}_{bc}\hat{G}^A(\varepsilon)\Big]\Big\} + b\leftrightarrow c, \tag{3.6}$$

$$\chi^{III}_{abc} = -\frac{e^3\hbar^2}{8\pi}\int[\mathrm{d}k]\int_{-\infty}^{\infty}\mathrm{d}\varepsilon f(\varepsilon)\mathrm{Im}\Big\{\mathrm{Tr}\Big\{\hat{v}_a\frac{\partial^2\hat{G}^R(\varepsilon)}{\partial\varepsilon^2}\hat{v}_{bc}\hat{G}^R(\varepsilon) + 2\hat{v}_a\frac{\partial}{\partial\varepsilon}\Big[\frac{\partial\hat{G}^R(\varepsilon)}{\partial\varepsilon}\hat{v}_b\hat{G}^R(\varepsilon)\Big]\hat{v}_c\hat{G}^R(\varepsilon)\Big\}\Big\} + b\leftrightarrow c, \tag{3.7}$$

$[\mathrm{d}k] = \frac{\mathrm{d}^n k}{2\pi}^n$ where n is the dimensionality. $\hat{v}_{ab} = \partial^b_k\partial^a_k\hat{\mathcal{H}}/\hbar^2$ and $\hat{v}_{abc} = \partial^c_k\partial^b_k\partial^a_k\hat{\mathcal{H}}/\hbar^3$ represent the tensor generalization of the velocity operator $\hat{v}_a = \partial^a_k\hat{\mathcal{H}}/\hbar$, where $\partial^a_k \equiv \partial/\partial k_a$. $\hat{v}_{abc}$ and $\hat{v}_{ab}$ are the cases for two-photon and three-photon processes, respectively. $\hat{G}(\varepsilon)$ is Green's function. $f(\varepsilon)$ is the Fermi distribution.

The first two terms, χ^{I}_{abc} and χ^{II}_{abc}, are the contributions from the Fermi surface. χ^{I}_{abc} depicts the triangular diagrams, and χ^{II}_{abc} describes the two-photon diagrams. χ^{III}_{abc} is completely determined by a single Green's function and is one order smaller than the other terms in the weak-disorder limit. Therefore, the Fermi sea contribution term χ^{III}_{abc} can be ignored for low-frequency transport. We can explicitly characterize the distinct mechanisms of nonlinear Hall conductivity in the diagrammatic approach by translating into the eigenstate basis. Figure 3 depicts diagrams of time-reversal symmetric systems governed by various mechanisms corresponding to semi-classical theory.

4 Zero field: Coulomb instabilities

Higher-order TIs [63–72] have recently drawn interest as generalizations of TIs [30, 73–83].

A 3D gapped bulk state may be found in the most

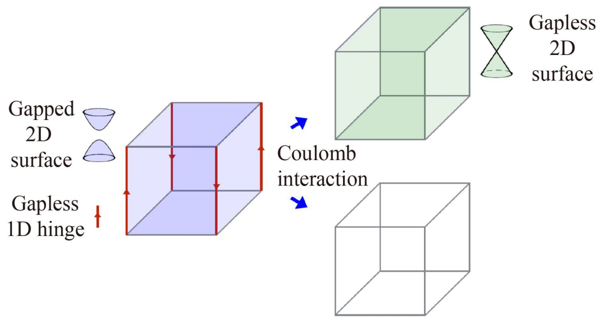

Fig. 4 The left diagram is a 3D second-order TIs. When Coulomb interaction exists, this system may transition to a TI or a trivial insulator. Reproduced from Ref. [20].

basic 3D second-order TIs. Gapped 2D surface states and gapless 1D hinge states are also present (Fig. 4). Noticed that the hinge states are protected by topology.

Experimental evidence for higher-order topology has been observed in bosonic systems, including acoustics [84–86], phononics [87], circuitry [88–90], and photonics [91–94]. We know that the stability of high-order TIs is very poor. There are two different topological phase transition (Fig. 4). First, second-order TIs undergo a topological phase transition to topological insulators when the Coulomb contact is present, and this transition is protected by inversion and time-reversal symmetries. This phenomenon indicates that when there is a Coulomb interaction, the second-order TI becomes unstable. Along with the phase transition, inversion and time-reversal symmetry also appear. The other phase transition, which is also induced by the Coulomb interaction, involves change from a second-order TIs to a trivial insulator. Both the surface and hinge modes vanish after this transition. And on the transition critical position, there is no time-reversal or inversion symmetries. However, these two emergent symmetries resurface when the phase transition is completed in the low-energy limit. It is interesting that there is not a general dynamical critical exponent for the transition. For each of the three scenarios, the dynamical critical exponent has a distinct value that is below 1. The four-band model is shown in Section 2.

In general, topological phase transitions from a higher-order TIs to a trivial insulator or a normal TI are accomplished by doping, as in studies using the candidate materials [70], $EuIn_2As_2$ [95], and $MnBi_2Te_4$ [96].

5 Zero field: The antiferromagnetic topological insulator's surface states

A TI has an insulator bulk and conductor surface states which are topologically protected [30, 81, 82, 97, 98]. The breaking of time-reversal symmetry will open a band gap in the surface states if we allow TIs to be doped with magnetic impurities [99–102], which is important for the realization of the QAHE. However, the QAHE can usually only be seen at low temperatures, as magnetic impurities invariably create disorder and inhomogeneity [103, 104]. The recently developed concept of the intrinsically magnetic TI suggests a promising strategy to increase the working temperature. One of the predicted candidate intrinsically magnetic TI materials is $MnBi_2Te_4$ [105–108]. However, the most recent experiments suggest that, in contrast to past predictions and observations [108–111], a bulk crystal of $MnBi_2Te_4$ may have gapless topological surface states. To solve this problem, beginning from a 3D model for $MnBi_2Te_4$ and considering magnetization's spatial distribution, we analytically build an 2D surface state's effective model.

The $\boldsymbol{k}\cdot\boldsymbol{p}$ approach yields results that are consistent with those of *ab initio* calculations,when the envelope function is used. The calculations of the surface states' distribution and depth of penetration show that the utmost edge two septuple layers are permeated by most surface states. The 3D Hamiltonian of $MnBi_2Te_4$ is shown in Section 2.3.

The localization of intralayer ferromagnetic order is described by odd-integer n, such that the greater the localization, the greater is n.

We can show that $E^{\pm}_{\text{surface}} = E_0 - Dk^2 \pm \sqrt{m^2+\gamma^2k^2}$ for states localized at the surface. This indicates that at the Γ point there will have a $2|m|$ gap opened by the surface states.

When n increases, there may have more localized intralayer ferromagnetic order and smaller effective magnetic moment m. The same happens when m_0 decreases. Therefore, our calculations imply that a considerably smaller and more localized intralayer ferromagnetic order may be the root of the diminished surface gap. It is significant that we discover that the penetration depth ξ (16.2 Å) is more than the septuple layer thickness (13.7 Å). This suggests that the second septuple layer has already been penetrated by the surface states.

In Ref. [21], a $\boldsymbol{k}\cdot\boldsymbol{p}$ model was derived for $MnBi_2Te_4$ thin films, and the Chern number was shown to oscillate between odd and even septuple layers, which is consistent with the nature of intrinsic antiferromagnetic TIs [106, 107]. Recent studies have revealed that the atomic magnetic moment of Mn is significantly lower than the theoretically expectation of $5\mu_B$ and $4.6\mu_B$, being about $3.8\mu_B$ in bulk of $MnBi_2Te_4$ and around $1.14\mu_B$ in thin films. This suggests that in actual materials, the intralayer ferromagnetic order shrinks significantly and becomes much more localized.

6 Zero field: Nonlocal surface transport

The hypothetical particle axion has not been seen in

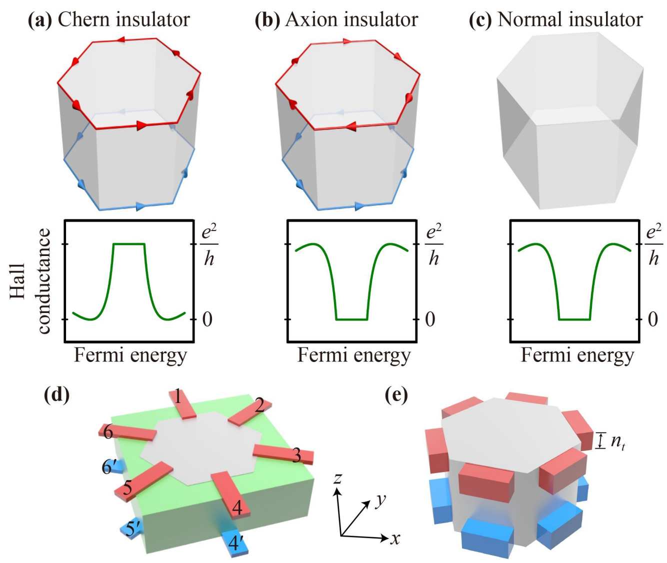

Fig. 5 For $MnBi_2Te_4$, **(a)** a Chern insulator is formed from odd septuple layers, **(b)** an axion insulator is formed from even septuple layers. **(c)** The normal insulator. **(d, e)** The nonlocal surface measuring device. The thickness of the thick electrodes is n_t. The phase of a $MnBi_2Te_4$ can be known by measuring its Hall conductance σ_{xy}. Reproduced from Ref. [22].

experiments but is thought to be necessary to solve the strong CP problem [112]. On its top and bottom surfaces, antiparallel chiral currents in the axion insulator are believed to be "half-quantized", which could result in the topological magnetoelectric effect [113–119] or a "half-quantized" surface Hall conductance [119–123]. Each current carries a quantized conductance $e^2/(2h)$ and the total measured conductance is 0. Unfortunately, the axion insulator has yet to be discovered experimentally because its signatures require extremely precise measurements and high device manufacturing precision. As shown in Figs. 5(a) and (b), the parallel chiral currents on the bottom and top surfaces of Chern insulator make it significantly different with the axion insulator. Optical measurements can be used to distinguish between the Chern and axion insulators. However, there is also zero Hall conductance in normal insulators [Fig. 5(c)], which makes it very difficult to identify signatures of the axion insulator.

A device made of the antiferromagnetic TI $MnBi_2Te_4$ may be used to measure nonlocal surface resistance to tell axion insulator apart from a normal insulator. We can use some classical theoretical approach to calculate the nonlocal surface transport [124–129]. The nonlocal resistances of a pair of surfaces are the same for odd layers. In contrast, the two surfaces' nonlocal resistancesusually differ for even layers, except when $p, q = 3, 6$. This means that both the Chern insulator in odd layers and the axion insulator in even layers exhibit unique nonlocal surface transport features. More significantly, the absence of chiral current in the normal insulator results in zero nonlocal resistance. As a result, the axion insulator has a special nonlocal resistance that sets it apart from other insulators.

Stacking septuple layers with out-of-plane magnetization results in the formation of $MnBi_2Te_4$. The magnetizations of adjacent septuple layers are in opposition. The even layers have opposite direct chiral currents on the bottom and top surfaces, satisfying the conditions for the formation of an axion insulator. In contrast to the Chern insulator and trivial insulator, the axion insulator exhibits significant nonlocal surface transport because of the chiral currents. As a result, the nonlocal surface transport offers an efficient way to find axion insulator.

The calculation in Ref. [22] shows that the thick electrodes, disorder and side-surfaces have little effect on nonlocal surface transport.

7 Weak field: Decays of Majorana oscillations

It is still difficult to identify and engineer Majorana bound states (MBSs) [130–134] for topological quantum computing [135–137]. A widely investigated candidate [138–152] for topological quantum computing is the Majorana zero mode in a superconductor–semiconductor nanowire [153, 154] because of its high tunability [155]. The MBSs are localized at the nanowire's two endpoints and are always found in pairs, which are presumed to have zero energy. However, the MBSs hybridize within a few micrometers in practical nanowires. According to the theory of Majorana oscillations, the hybridization energy E_0 fluctuates depending on the wire length, chemical potential, or Zeeman energy [156–158].

Recent research on islands of nanowires has revealed that E_0 oscillates as the magnetic field increases. After an overshoot, the oscillation's amplitude either decreases or disappears [149, 159–162], while the oscillation period increases [159, 162]. These behaviors, however, contradict the existing theories [157] of MBSs, which predict an increase in both the oscillation amplitude and period.

The oscillation pictures seen in the studies, including the increase in period and the decrease in amplitude, may be explained by a simple but reasonable hypothesis that there is a steplike distribution spin–orbit coupling along the nanowire [Figs. 6(b)–(d)].

The blue lines in Fig. 6 plot the results of numerical simulations calculated utilizing three different model parameter settings [23].

In addition to reproducing the declining amplitude, the simulations also capture the increasing oscillation time [Fig. 6(c)], anticrossing [Fig. 6(d)], and lowest-energy crossover [Fig. 6(b)], all of which are in agreement with the experiments. If the magnetic field is increased further, the oscillation amplitude may start to increase

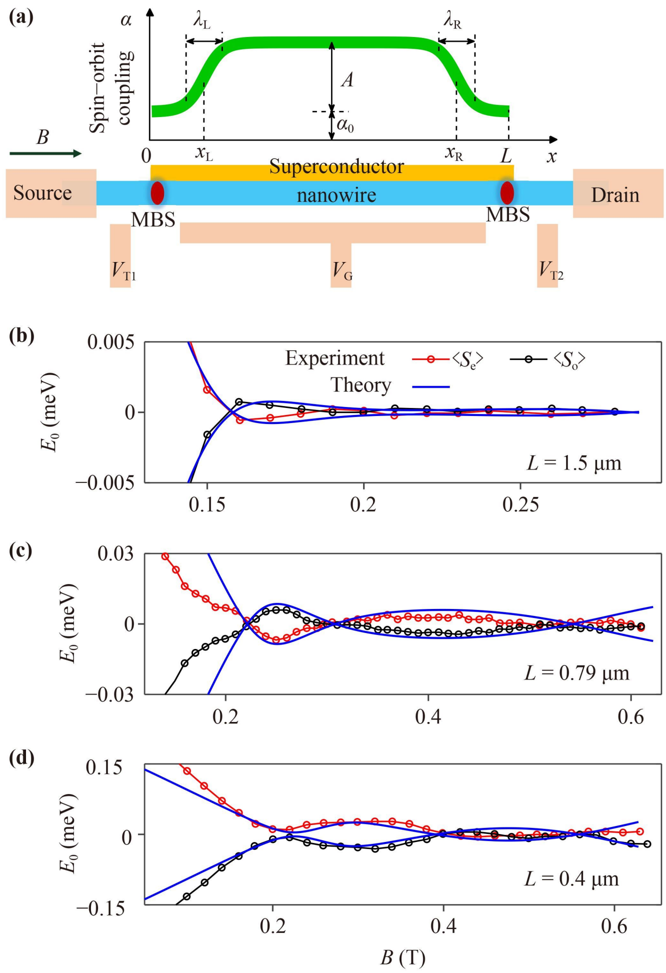

Fig. 6 **(a)** The superconductor–semiconductor nanowire island [149, 159–162]. **(b–d)** As a function of the B, the hybridization energy E_0 oscillates in experiments with a rising period and diminishing amplitude. However, these experimental observations contradict the theory of MBSs, which predicts that E_0 oscillates with increasing amplitude induced Zeeman energy V_Z [157]. Reproduced from Refs. [23, 159].

rather than decrease as superconductivity is suppressed under such conditions.

It is not just MBSs that exhibit these decaying oscillations. The possibility of using the same device to host Andreev bound states has been proposed [163–166].

8 Strong field: One-sided hinge states

Great efforts have been made to find a quantum Hall effect in dimensions other than two [28, 167–193] since the quantum Hall effect was discovered [194, 195]. Fermi arcs and Weyl nodes from opposite surfaces can form a "Weyl orbital", a mechanism that enables the magnetic field to drive the cyclotron motion and the 3D QHE in topological semimetals [65, 196] [Figs. 7(a)–(c)].

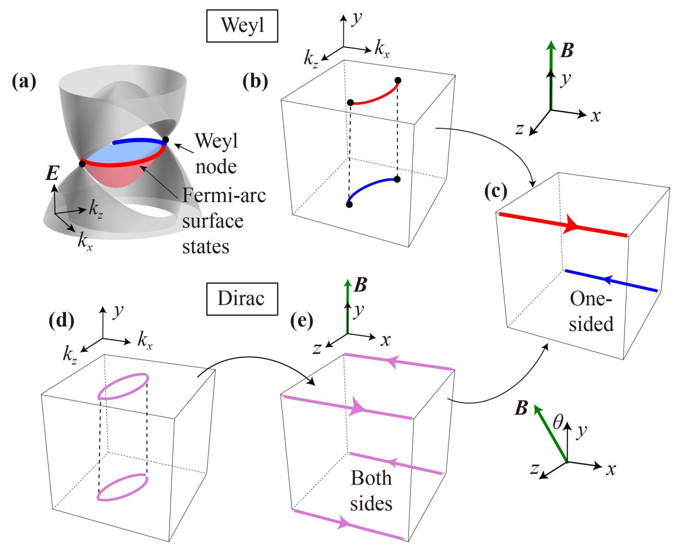

Fig. 7 **(a)** Energy band schematic for a Weyl semimetal. **(b, c)** The schematic of Fermi-arc surface states and corresponding one-sided hinge states under magnetic field $\boldsymbol{B}$. **(d, e)** The schematic of hinge states on both sides in Dirac semimetals. We have shown that in Dirac semimetal the Fermi energy (Fig. 8) and slanted magnetic field may produce one-sided, highly tunable hinge states. Reproduced from Ref. [24].

This 3D QHE is distinguished by the one-sided hinge states. As shown in Fig. 7(c), one state is located on side of the bottom surface and the other one on the opposite side of the top surface. These states were not observed in any previously studied systems [63, 64, 66–71, 87–90, 197–222]. Due to stringent symmetry requirements, it is very difficult to experimentally detect higher-order TIs. On the other hand, the one-sided hinge states can both explain the 3D QHE and possibly make it easier to detect higher-order topological states. Only the topological semimetal Cd_3As_2 have shown evidence of the QHE [223–228], and its mechanism is still a matter of discussion. Furthermore, time-reversal symmetry produces two-sided hinge states rather of the anticipated one-sided ones since two Weyl semimetals with time-reversed symmetry constitute Cd_3As_2 [Figs. 7(d–e)].

In this section, we introduce the realization of the one-sided hinge states in tilted magnetic fields in Dirac semimetals such as Cd_3As_2, as shown in Figs. 7(e)–(c). In experiments, we get a sample grown along [110] direction and then numerically calculate wave function distributions and energy spectra (Fig. 8). The slab exhibits desired hinge states, the placement of which can be tuned via the Fermi energy E_F and magnetic field's angle θ.

Figure 8 shows the wave function distributions and energy spectra of Cd_3As_2. $B_y = 15\,\mathrm{T}$. Here we choose three tilt angles: $\theta = 0, \pm 5°$. In each scenario, the gap near $E = 0$ appears in the energy spectrum. The hinge states appear, as illustrated by the pink dashed line in

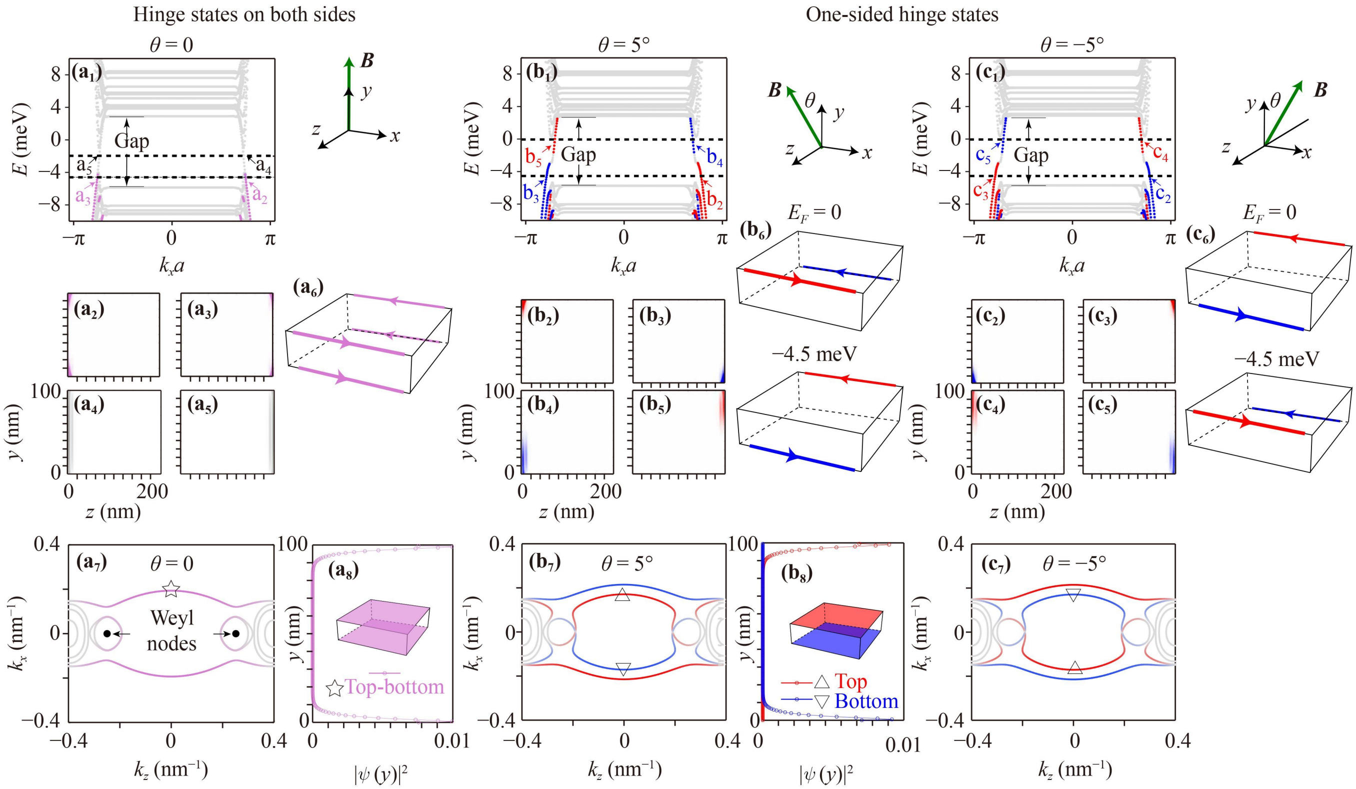

Fig. 8 **(a_1)** The Dirac semimetal's energy spectrum, when $B_y = 15$ and ($\theta = 0$). **(a_2–a_5)** The distributions of wave functions for the states indicated in (a_1) by horizontal dashed lines. **(a_6)** illustrates the position hinge states at $E_F = -4.5$ meV. **(a_7)** shows the Fermi surface when only taking the magnetic field's Zeeman effect into account. **(a_8)** shows the state indicated by the star's wave function dispersion in (a_7). (b_1–b_8) $\theta = 5°$. (c_1–c_7) $\theta = -5°$. Reproduced from Ref. [24].

Fig. 8(a_1). The slab's four hinges move in opposing orientations along the opposing flank surfaces [Figs. 8(a)]. Additionally, the gray points represent the chiral states on the flank surfaces and the Landau levels on the bottom and top surfaces.

Next, we discuss the case of a tilted magnetic field. When we let angle to 5°, the Fermi suface is inside of the Landau-level gap [Figs. 8, Part (b)]. For $E_F =$ –4.5 meV, the red and blue lines illustrate the hinge states with well-localized. The states are shifted to opposing flanks, while $E_F = 0$ meV. Because the hinge states and the side-surface chiral states may couple with each other, the hinge states will not localized very well at $E_F = 0$. If we change the sign of θ, the hinge states shift to the other flank, as illustrated in Figs. 8(c_1)–(c_6).

The aforementioned hinge states' evolution may be explained using the Fermi arcs, which are controllable by the Zeeman fields. The hinge states are the edge states of the Fermi arc surface states' Landau levels under magnetic fields. The blue and red lines are the Fermi arcs in Fig. 7, which are the cornerstone of the the one-sided hinge states and 3D QHE. When $\theta = 0$, on both the topbottom and top surfaces, Fermi arcs are equally dispersed. Weyl semi-metals with time reversal symmetry are coupled by Zeeman coupling Δ_y. The results of this coupling are illustrated in Fig. 8(a_7). This even distribution takes rise to four hinge states on different flanks, as shown in Fig. 8(a_6). However, when the angle have ±5°, the hinge states are produced by the decoupling of Fermi arcs on opposing surfaces by the z direction Zeeman splitting Δ_z.

Calculations prove that the one-sided hinge states need a big enough Landau-level gap to be protected, and this Landau-level gap depends on the strength of the Zeeman coupling.

9 Strong field: Helical edge states and QHE

Since the find of the QHE in 2DEG [41, 195], there have been considerable efforts to generalize this exotic phase in higher dimensions matter [167, 168, 186], systems without magnetic fields [100, 229], and the nonlinear response regime [17–19, 45, 46, 59]. In the Cd_3As_2, which is a topological Dirac semimetal, quantized conductance plateaus have recently been seen [223, 224, 226–228, 230–233]. One mechanism of the QHEt, introduced in Section 8, depends on Fermi-arc surface states [24, 65, 196]. Table 1 summarizes the results of studies of the QHE in 3D topological semimetals and the mechanistic

Table 1 Recent experimental studies of the QHE in the topological semimetal Cd_3As_2: slab growth direction, thickness, and mechanistic explanation.

Ref.	Crystal orientation	Thickness (nm)	Analysis
[231, 226]	[112]	12–23, 35	Bulk subbands
[234, 227]	[112]	20, 38–43	Surface states
[233, 224]	[112]	80, 100	Mixed Fermi arcs
[230, 232]	[112]	55–71, 80–150	Weyl orbit
[223]	[001]	45–50	Topological insulator type surface states
[235]	[010]	150–2000	Weyl orbit

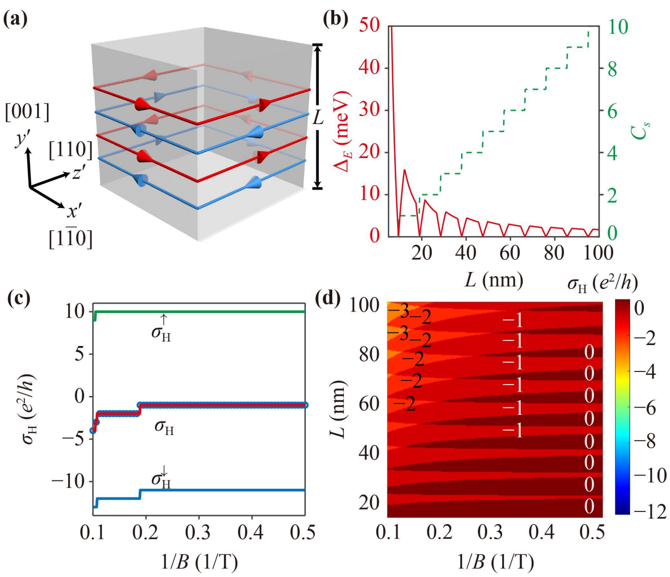

Fig. 9 **(a)** The schematic of helical edge states. The different colour represent different spin polarizations and directions of propagation. **(b)** The green line shows the spin Chern number C_s. The red line is the confinement-induced energy gap. **(c)** The Hall conductance. **(d)** The Hall conductance as a function of thickness and field. Reproduced from Ref. [25].

explanations proposed therein.

We propose a novel mechanistic explanation of the QHE in topological semimetals. First, we note that there are three crystallographic orientations that are easily accessible to experiment and are often studied in the Dirac semimetal Cd_3As_2 slabs. We introduce the numerical calculation of the Hall conductance in these three orientations. For the thick plate grown in [001] orientation, the amount of the quantized Hall conductance rises with the field due to the Zeeman splitting of the helical edge states (Fig. 9). In contrast, as a result of the Fermi-arc 3D QHE, the Hall plateaus for the thick plate grown along the [110] orientation decline as the magnetic field increases [65]. Considering these observations, it is possible to interpret the conductance in the slab along the [112] orientation as a clash between helical edge states and the Fermi-arc surface states. In this situation, the Hall plateaus decrease while the field is weak and increase while the field become larger.

10 Extremely strong field: Kramers Weyl semimetal's negative magnetoresistance

Negative magnetoresistance is a very important physical phenomenon. Randomly oriented ferromagnetic domains in magnetic materials reduce electron tunneling and increase resistance. A negative magnetoresistance can result from a magnetic field that reduces the resistance and aligns the domains. Negative magnetoresistance [236] is uncommon because electrons are prevented from traveling forward by the Lorentz force in non-magnetic materials. A well-known negative magnetoresistance case is weak localization [237], which can only occur at very low temperatures as it is caused by quantum interference. At higher temperatures, negative magnetoresistance in non-magnetic TIs [238–243] and semimetals [6, 244–255] has recently sparked great attention. The chiral anomaly is commonly thought to be the source of the negative magnetoresistance in topological semimetals [256–258]. In TIs, it has also been discovered that negative magnetoresistance is connected to the nontrivial Berry curvature distribution induced anomalous velocity [7].

With the current-parallel magnetic field, a recent experiment on the β-Ag_2Se [38] demonstrated a negative magnetoresistance. Kramers Weyl semimetals have time-reversal invariant momenta in the Brillouin zone that hold Weyl nodes in place, and β-Ag_2Se is a candidate material for this type of system [259, 260]. Given that they are present in all chiral crystals, the Kramers Weyl nodes have handedness [260]. At a magnetic field of about 9 T, a negative magnetoresistance of about -20% was noted in β-Ag_2Se. The system reached the quantum limit under that powerful magnetic field. In this situation, the Fermi energy can only be crossed by the lowest Landau band, and the scattering mechanisms have a subtle impact on the magnetoresistance [10, 11, 261].

In this section, a theory for a Kramers Weyl semimetal's longitudinal magnetoresistance in the quantum limit is presented. We begin with a single Kramers cone model with and calculate the conductivity using the Kubo formalism while taking Gaussian potentials and impurity scattering into consideration. Results demonstrate that the resistance has a $1/B$ dependency in the quantum limit when disorder are present, resulting in a negative magnetoresistance.

Now for the $\nu = 0$ band, the longitudinal conductivity is

$$\sigma_{zz,0} = \frac{e^2}{h}\frac{\epsilon\hbar v_{\mathrm{F}}^0}{\pi^2 n_{\mathrm{imp}} e^2 \ell_B^4}. \tag{10.1}$$

We know that $1/\ell_B^4 \propto B^2$ and the velocity along the z-direction $v_F^0 \propto 1/B$. Then, we can obtain the dependency between $\sigma_{zz,0}$ and magnetic field B:

$$\sigma_{zz,0} \propto B. \tag{10.2}$$

As there is no Hall effect under a parallel B, the resistance $\rho_{zz,0}$ is equal to the conductivity's inverse. Get,

$$\rho_{zz,0} \propto \frac{1}{B}, \tag{10.3}$$

and it indicates that the Kramers–Weyl cone has a negative longitudinal magnetoresistance in quantum limit.

If we consider a Gaussian scattering potential, the conductivity is

$$\sigma_{zz,0}^{\mathrm{G}} = \frac{e^2}{h}\frac{(\hbar v_{\mathrm{F}}^0)^2(2d^2+\ell_B^2)}{V_{\mathrm{imp}}\ell_B^2} e^{2(2d^2+\ell_B^2)(k_{\mathrm{F}}^0)^2}. \tag{10.4}$$

According to $k_{\mathrm{F}}^0 \propto v_{\mathrm{F}}^0 \propto 1/B$, $\sigma_{zz,0}^{\mathrm{G}}$ will decrease as B increases. This relationship indicates when the Gaussian scattering potential is present there is no negative magnetoresistance. We demonstrate that a negative magnetoresistance requires a screened Coulomb scattering potential.

11 Extremely strong field: Non-saturating quantum magnetization

The low-energy states of electrons in topological materials may be seen as a group of quasiparticles adhering to various representation of the Dirac equation [262–266]. The Weyl fermion, a three-dimensional massless quasi-particle, was found in Dirac and Weyl semimetals [36, 267–273]. Numerous unexpected properties of these massless quasiparticles, including surface Fermi arcs, monopoles, and linear energy dispersion, are promised by Weyl semimetals' distinctive topological nature [274–276]. In particular, the Weyl fermions' 0th Landau bands in strong magnetic fields are entirely chiral modes [256, 257, 277]. As discussed in Section 10, a negative longitudinal magnetoresistance, which is the hallmark of the chiral anomaly in quantum field theory, is anticipated to be present in the 1D chiral Landau bands [278]. However, in Section 10 we present the fact that the magnetoresistance also depends on the property of impurity scattering in a sophisticated manner in the quantum limit and cannot provide information on the spectrum of the quasiparticles deterministically [10, 11, 261].

The magnetic response of electrons, in comparison, are considerably easy as they do not interact with impurity scattering. In fact, the derivatives of the thermodynamic potential of the electrons with respect to the magnetic field are all that need to be considered to determine them, and can be applied to study the characteristics of Fermi surface [279–281].

For this section, we propose a technique for using the magnetic responses of electrons to detect relativistic quasiparticles. When all of the other Landau bands have departed from the Fermi surface, we concentrate on the zeroth Landau band's magnetic response under a sufficiently large magnetic field. Under these extreme situations, the magnetic response of the crossing bands is noticeably different from that of ordinary parabolic bands. Because TaAs hosts well-defined Weyl quasi-electrons which help to demonstrate the unique features of such a material, it was selected for a prototype topological semimetal. We demonstrate that beyond the quantum limit, the parallel magnetizations ($M_{//}$) and effective transverse (M_T) of TaAs are quasi-linearly field-dependent. The non-relativistic quasiparticles'magnetic responses are different from non-saturating magnetic responses, in agreement with our calculations.

The magnetic response pictures for non-relativistic and relativistic electron systems are compared first. Figures 10(a) and (b) depict the band diagrams for holes and non-relativistic electrons. When the field is increased, the Landau bands gradually depart from E_F [Fig. 10(b)], which causes $M_{//}$ to oscillate around zero and M_T to decrease with increasing field strength [Figs. 10(c) and (d)]. This process continues until all the Landau bands with the exception of the lowest have exited E_F. Note that as the system go in to the quantum limit, the change in E_F under a strong magnetic field becomes non-negligible. If we fixed E_F, the 0 point energy will put up the zeroth Landau band above Fermi energy, which will cause $M_{//}$ and M_T to disappear (above the critical magnetic field), as shown by the red dotted lines in Figs. 10(c) and (d). If we fixed N_c, no matter the magnitude of the magnetic field increase, E_F will be pinned at the margin of the zeroth Landau band. As illustrated by the blue lines in Figs. 10(c) and (d), $M_{//}$ will saturate under this constraint, and M_T will remain constant. Consequently, due to band dispersion of non-relativistic, M_T and $M_{//}$ are unchanging in the quantum limit. For 3D massive bulk systems, including InSb [281–283], sulfur-doped Bi_2Te_3, and Bi, the signature of the saturated M_T and $M_{//}$ in the quantum limit has been observed.

In contrast, because of the relativistic spectrum and band inversion, gapless Weyl fermions provide a distinct contribution to the magnetization [Figs. 10(e) and (f)], which in low magnetic field strengths causes $M_{//}$ and M_T to oscillate around a mean value, as illustrated in Figs. 10(g) and (h). When the remaining Landau bands exit Fermi energy, both chiral modes contribute to the magnetic response [Figs. 10(f)], resulting in non-saturating M_T and $M_{//}$ in a large magnetic field. The nature of relativistic electrons in the quantum limit is responsible for the fundamental difference in magnetic responses.

Because in the quantum limit the linear non-saturating magnetization deviates from Landau's theory of magne-

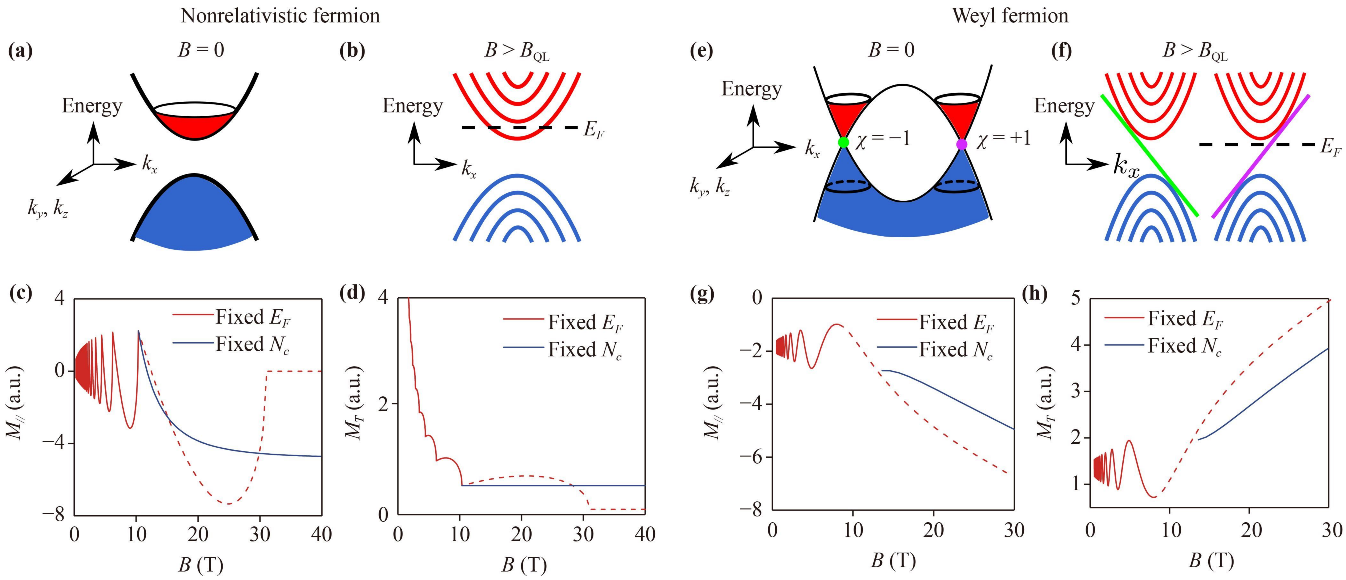

Fig. 10 **(a–d)** Non-relativistic fermion. **(a)** The energy bands without magnetic field. **(b)** The Landau bands. **(c)** Parallel magnetization $M_{//}$. **(d)** Effective transverse magnetization (M_T). **(e–h)** Schematic of Weyl fermion same with (a–d). Reprocuced from Ref. [27].

tization for classical electrons, it is of special importance. Semimetals with overlapped parabolic hole and electron bulk bands have never demonstrated such a property under large magnetic fields. The linear energy dispersion of Weyl fermions' 0th Landau band has a distinctive magnetic response in the quantum limit, as shown by our calculations and measurements. We stress once more that the explanation and calculations are based on a single-particle case. Future study will be interesting in examining how our theory of one-particle physics applies to many-body phenomena like excitons.

12 Extremely strong field: CDW mechanism of 3D QHE

It is difficult to perceive the QHE in 3D systems because the Landau levels combine into a collection of 1D bands known as Landau level dispersion, which have momentum along the direction of the magnetic field. However, the QHE is often observed in 2D systems because the interior becomes metallic as a result of the Fermi energy always crossing particular Landau bands, which covers up the edge states' quantiztion [284]. One of the best-known theories for the 3D QHE depends on the possibility that the CDW creates gaps in the 1D Landau band and makes the bulk non-conducting. To create a 3D QHE in real space, the 3DEG is divided by the CDW into decoupled 2D quantum Hall layers. Lately, the CDW mechanism of the 3D QHE has been reported in $ZrTe_5$ [181]. In contrast to earlier instances, in $ZrTe_5$, the 1D band of Landau levels, which is heavily reliant on the magnetic field, is where the CDW forms.

Here, we introduce a theory for the CDW mechanism of the 3D QHE. The most important features experimentally observed in $ZrTe_5$ are quantitatively captured by the theory. Instead of e–e interactions, we show that e–ph interactions are more important in the development of the CDW. We take the non-Ohmic I–V relation and derive the e–ph coupling constant. We draw attention to a magnetic field-tunable crossover between incommensurate and commensurate CDW. More crucially, the theory accounts for an uncommon but experimentally accessible case that using a single magnetic field, one may tune both an order parameter along one direction and a topological Chern number in the other two.

The gap equation established by $\partial E_g/\partial|\Delta| = 0$ is used to calculate the self-consistent CDW order parameter. The ground-state energy $E_g \equiv \langle \hat{H}_m \rangle$ is found to be

$$E_g = \sum_{\boldsymbol{k}} (E_{k_z} - E_F)\Theta(E_F - E_{k_z}) + \frac{|\Delta|^2 V}{g_{2k_F}}, \qquad (12.1)$$

where $\Theta(x)$ is the step function, E_g includes phonon part, $\hat{H}_m = \sum_{\boldsymbol{k}} \hat{\Psi}^\dagger_{\boldsymbol{k}} \mathcal{H}^{0+}_{k_z} \hat{\Psi}_{\boldsymbol{k}} + |\Delta|^2 V/g_{2k_F}$, $\hat{\Psi}_{\boldsymbol{k}} \equiv (\hat{d}_{\boldsymbol{k}+}, \hat{d}_{\boldsymbol{k}-})^{\mathrm{T}}$. The coupling $g_{2k_F} = e^2/\{2\epsilon[(2k_F)^2 + \kappa^2]\}$ for e–e interactions and $g_{2k_F} = g_0/[(2k_F)^2 + \kappa^2]^2$ for e–ph interactions with the coupling constant g_0. The mean-field phonon Hamiltonian is able to account for the second positive term.

Symbol of the fractional QHE have been seen at greater magnetic fields [181]. The plateau-like Hall resistivity at lower magnetic fields were also experimentally observed, suggesting the coinstantaneous CDW phase composed of numerous bands. In layered materials such as $HfTe_5$, TaS_2, and $NbSe_3$, the CDW mechanism of the 3D QHE can also be accomplished.

13 Extremely strong field: 3D metal–insulator transitions

The transition from metal to insulator induced by magnetic field [285–287] have been widely researched in 2D systems [285–301], but a 3D theory remains absent. Recent studies illustrate metal–insulator transitions in 3D systems may due to the presence of magnetic fields [181, 302–305] with quantum phase transition features [306, 307], specifically under strong magnetic field of a TI [181, 305].

This section, we introduce a scaling theory for the transition from metal to insulator of a 3D TI at strong magnetic fields. Our theory and recent experiments are in great agreement [181]. The phase transition is determined by the critical exponents of general relations that correspond to distinct instabilities and universal classes [307–314]. We determine the correlation length exponents ν and dynamical critical exponents z for the candidate instabilities using a renormalization-group calculation. We construct scaling relations connecting the magnetic field, temperature, and resistivity, which are represented by a critical exponent ξ. By contrasting our results with the experimentally obtained $\xi = 5.5$ [181], we come to the conclusion that the insulating ground state is a CDW driven by backscattering disorder, strong e–e interactions, and e–ph interactions. By fitting the correlation length exponent and dynamical critical exponent, we additionally offer the experiment of current-scaling for additional demonstration.

There are two fixed points for a system that exclusively has e–e and e–ph interactions. In such system, the critical exponent is $\xi = 3z\nu_\beta = 1.5$. This number is much lower than the experimental value $\xi = 5.5$ [181]. Therefore, the experimental metal–insulator transitions cannot be induced by the simultaneous presence of e–e and e–ph interactions without disorder [181].

When considering disorder of backscattering, the fixed points are (i)$_b$ $(u_*, \beta_*, \Delta_b^*) = (0, 0, 0)$; (ii)$_b$ $[0, (1 + 1/\gamma)^2, 0]$; (iii)$_b$ $(0, 0, 1/4)$; and (iv)$_b$ $(1/2, 0, 1/2)$. Due to their various critical exponents, they belong to four separate universality classes. There is a demarcation line in the u–Δ_b plane, as illustrated in Fig. 11(c), where u flows to infinity on the right, suggesting a CDW driven by e–e interactions. Meanwhile, the system reaches a steady zero-valued e–e coupling and a fixed point of finite disorder on the left. The deed of u does not qualitatively alter when including e–ph interactions, as demonstrated in Fig. 11(d). In the presence of limited backscattering disorder and negligible e–e coupling, there will be a critical point (iii)$_b$ for a CDW induced by e–ph interactions. For this universality class, the dynamical critical exponent is calculated as $z = 1 + 2\Delta_b^* = 1.5$. Thus, we obtain $\xi = 3z\nu_\beta = 4.5$ for the scaling of resistivity, which nearly matches the experimental number 5.5 [181].

Both u and β are volatile when close to fixed point

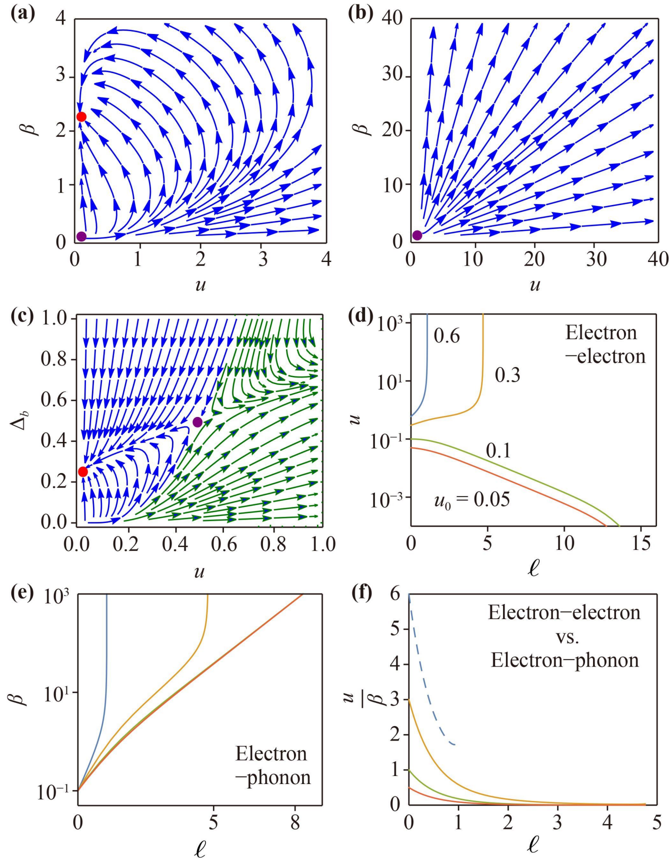

Fig. 11 **(a)** $\gamma = 2$, **(b)** $\gamma = 0.002$. The effective electron–phonon and electron–electron interactions are measured by β and u, respectively. $\gamma = |v_b/v_F|$. **(c)** The diagram without electron–phonon coupling. This picture shows double non-Gaussian points at $(u_*, \Delta_b^*) = (0, 1/4)$ and $(1/2, 1/2)$. The red line separates between a Wigner crystal and a disordered metal with zero electron–electron interaction on the left. **(d–f)** u, β, and u/β as a functiong of ℓ for various u starting values. Reproduced from Ref. [29].

(iv)$_b$ and rise without bounds while the starting value of u is very large. For the Peierls phase transition or Wigner crystal, fixed point (iv)$_b$ is a multicritical point. The ratio of u to β rapidly declines and eventually vanishes if its starting value is too low, as shown in Fig. 11(e), demonstrating that the Peierls phase transition occurs first. The Wigner crystal, on the other hand, always appears first when the starting value of u is large enough, as indicated by the dotted line in Fig. 11(f).

The critical behaviors and gap sizes of these two phase transitions are distinct, although they both result in CDWs [315, 316].

14 Remarks and perspective

Nonlinear optics and the nonlinear Hall effect are very different from one another. Light has a frequency of about 10^{14} Hz in nonlinear optical phenomena [317], for instance, the second-harmonic generation and photovoltaic effect, which is high enough to cause interband transitions in semiconductors. Contrarily, in nonlinear Hall measurements, the frequency is too low to result in interband transitions, preventing the pertinent physical effects from manifesting beyond the Fermi surface. The research of topological physics and quantum transport is pushed into the nonlinear response regime by the nonlinear generalization of the Hall effects, opening up a extensive prospect of intriguing possibilities for future study. Our understanding of the nonlinear Hall effect has come a long way, but there are still many unanswered problems and difficulties to be overcome, such as identifying additional materials that have significant NHE. Additionally, as the NHE shown in experiments typically exist at high temperature, the effect of temperature warrants theoretical investigation.

The research for higher-order TIs will depend on Coulomb interactions, even if these interactions are weak. We have created a theory in $BiTl(S_{1-\delta}Se_{\delta})_2$ [318] analogous to that explaining the transition between TIs and trivial insulators by keeping the parameter values at the cutoff and observing their behaviour at a certain low-energy scale. Changes in the parameters' starting values correspond to changes in the parameters on the specific energy scale that is related to the experiment. Hence, the phase transitions between a higher-order TI and a trivial insulator or a TI are experimentally achievable via doping, such as with the candidate materials Bi [70], $EuIn_2As_2$ [95], and $MnBi_2Te_4$ [96].

The assumption that the intralayer ferromagnetic order becomes significantly lesser and more localized in actual materials is supported by a number of experimental results. In recent experiments, the diminution for the intralayer ferromagnetic order has been demonstrated such as the example $MnBi_2Te_4$ in Section 5 [105, 107, 109, 319, 320]. Another interesting thing is what we talked about non-uniform spin–orbit coupling [321]. One is the steplike distribution spin–orbit coupling. The localized zero-energy Andreev bound states in the quantum dot are produced in the non-uniform case by connecting a spin–orbit-coupled quantum dot to a nanowire with zero spin–orbit coupling.

In large magnetic field, we anticipate that the Aharonov–Bohm effect be used to probe the one-sided hinge states, such as in a Fabry–Pérot interferometer [322]. By studying the quantum Hall effect in various growth directions in topological semimetals, we may learn to identify the QHE caused by the helical edge states and bulk subbands by measuring the nonlocal bulk transport, as demonstrated in Section 6.

Since it goes beyond Landau theory of magnetization for classical electrons, the linear non-saturating magnetization in the quantum limit is particularly intriguing [323]. Topological materials with relativistic quasiparticles that have recently emerged for prospective applications generally occur small Fermi surfaces in which quantum limit may be attained in a permanent magnetic field. It is difficult to identify the relativistic nature of quasiparticles using electrical transport and spectroscopic techniques. Magnetization can offer a way to identify relativistic quasiparticles in emerging matters. It will be very interesting to see how the one-particle physics theory described in Section 11 may be used to explain many-body effects like excitons [324].

Signatures of the fractional QHE have been seen at higher magnetic fields [181, 325]. Plateau-like behavior has also been experimentally observed in the Hall resistivity at lower magnetic fields [181], indicating a simultaneous CDW phase composed of multiple bands. Layered structures like $HfTe_5$, TaS_2, and $NbSe_3$ might also be used to realize the CDW mechanism of the 3D QHE. Additionally, CDWs might be studied using X-ray diffraction [326–329], although the use of X-ray equipment in the presence of a strong magnetic field is difficult.

In Section 13, although we use the experiments in Ref. [181] as a specific point of comparison, our theory may be used to explain various 3D metal–insulator transitions from metal to insulator that occur in large magnetic fields. Laterly, it was discovered that the field-driven transition from metal to insulator in β-Bi_4I_4 [329] had $\xi = 6.5$, demonstrating the broad applicability of our theory. However, our theory cannot explain 3D metal–insulator transitions of spin-correlated systems induced by magnetic fields [302–304], which remains a challenging problem for future research.

Acknowledgements We thank helpful discussions with Haipeng Sun and Rui Chen. This work was supported by the National Key R&D Program of China (No. 2022YFA1403700), the National Natural Science Foundation of China (No. 11925402), Guangdong province (Nos. 2020KCXTD001 and 2016ZT06D348), and the Science, Technology and Innovation Commission of Shenzhen Municipality (Nos. ZDSYS20170303165926217, JAY20170412152620376, and KYTDPT 20181011104202253). The numerical calculations were supported by Center for Computational Science and Engineering of SUSTech.

References

1. H. Z. Lu and S. Q. Shen, Quantum transport in topological semimetals under magnetic fields, *Front. Phys.* 12(3), 127201 (2017)
2. H. P. Sun and H. Z. Lu, Quantum transport in topological semimetals under magnetic fields (II), *Front. Phys.* 14(3), 33405 (2019)
3. X. B. Qiang and H. Z. Lu, Quantum transport in topological matters under magnetic fields, *Acta Phys. Sin.* 70(2), 027201 (2021)
4. H. Z. Lu and S. Q. Shen, Weak antilocalization and localization in disordered and interacting Weyl semimetals, *Phys. Rev. B* 92(3), 035203 (2015)
5. X. Dai, H. Z. Lu, S. Q. Shen, and H. Yao, Detecting

monopole charge in Weyl semimetals via quantum interference transport, *Phys. Rev. B* 93, 161110(R) (2016)
6. H. Li, H. T. He, H. Z. Lu, H. C. Zhang, H. C. Liu, R. Ma, Z. Y. Fan, S. Q. Shen, and J. N. Wang, Negative magnetoresistance in Dirac semimetal Cd_3As_2, *Nat. Commun.* 7(1), 10301 (2016)
7. X. Dai, Z. Z. Du, and H. Z. Lu, Negative magnetoresistance without chiral anomaly in topological insulators, *Phys. Rev. Lett.* 119(16), 166601 (2017)
8. C. Li, C. M. Wang, B. Wan, X. Wan, H. Z. Lu, and X. C. Xie, Rules for phase shifts of quantum oscillations in topological nodal-line semimetals, *Phys. Rev. Lett.* 120(14), 146602 (2018)
9. C. M. Wang, H. Z. Lu, and S. Q. Shen, Anomalous phase shift of quantum oscillations in 3D topological semimetals, *Phys. Rev. Lett.* 117(7), 077201 (2016)
10. H. Z. Lu, S. B. Zhang, and S. Q. Shen, High-field magnetoconductivity of topological semimetals with short range potential, *Phys. Rev. B* 92(4), 045203 (2015)
11. S. B. Zhang, H. Z. Lu, and S. Q. Shen, Linear magnetoconductivity in an intrinsic topological Weyl semimetal, *New J. Phys.* 18(5), 053039 (2016)
12. C. M. Wang, H. P. Sun, H. Z. Lu, and X. C. Xie, 3D quantum Hall effect of Fermi arcs in topological semimetals, *Phys. Rev. Lett.* 119(13), 136806 (2017)
13. Y. Chen, H. Z. Lu, and X. C. Xie, Forbidden backscattering and resistance dip in the quantum limit as a sig nature for topological insulators, *Phys. Rev. Lett.* 121(3), 036602 (2018)
14. C. L. Zhang, S. Y. Xu, C. M. Wang, Z. Lin, Z. Z. Du, C. Guo, C. C. Lee, H. Lu, Y. Feng, S. M. Huang, G. Chang, C. H. Hsu, H. Liu, H. Lin, L. Li, C. Zhang, J. Zhang, X. C. Xie, T. Neupert, M. Z. Hasan, H. Z. Lu, J. Wang, and S. Jia, Magnetic tunnelling induced Weyl node annihilation in TaP, *Nat. Phys.* 13(10), 979 (2017)
15. Z. Du, C. Wang, H. P. Sun, H. Z. Lu, and X. Xie, Quantum theory of the nonlinear Hall effect, *Nat. Commun.* 12(1), 5038 (2021)
16. Z. Du, H. Z. Lu, and X. Xie, Nonlinear Hall effects, *Nat. Rev. Phys.* 3(11), 744 (2021)
17. Z. Du, C. Wang, S. Li, H. Z. Lu, and X. Xie, Disorder induced nonlinear Hall effect with time-reversal symmetry, *Nat. Commun.* 10(1), 3047 (2019)
18. Q. Ma, S. Y. Xu, H. Shen, D. MacNeill, V. Fatemi, T. R. Chang, A. M. Mier Valdivia, S. Wu, Z. Du, C. H. Hsu, S. Fang, Q. D. Gibson, K. Watanabe, T. Taniguchi, R. J. Cava, E. Kaxiras, H. Z. Lu, H. Lin, L. Fu, N. Gedik, and P. Jarillo-Herrero, Observation of the nonlinear Hall effect under time-reversal symmetric conditions, *Nature* 565(7739), 337 (2019)
19. Z. Z. Du, C. M. Wang, H. Z. Lu, and X. C. Xie, Band signatures for strong nonlinear Hall effect in Bi layer WTe_2, *Phys. Rev. Lett.* 121(26), 266601 (2018)
20. P. L. Zhao, X. B. Qiang, H. Z. Lu, and X. C. Xie, Coulomb instabilities of a three-dimensional higher-order topological insulator, *Phys. Rev. Lett.* 127(17), 176601 (2021)
21. H. P. Sun, C. M. Wang, S. B. Zhang, R. Chen, Y. Zhao, C. Liu, Q. Liu, C. Chen, H. Z. Lu, and X. C. Xie, Analytical solution for the surface states of the antiferromagnetic topological insulator $MnBi_2Te_4$, *Phys. Rev. B* 102(24), 241406 (2020)
22. R. Chen, S. Li, H. P. Sun, Q. Liu, Y. Zhao, H. Z. Lu, and X. C. Xie, Using nonlocal surface trans port to identify the axion insulator, *Phys. Rev. B* 103(24), L241409 (2021)
23. Z. Cao, H. Zhang, H. F. Lü, W. X. He, H. Z. Lu, and X. C. Xie, Decays of Majorana or Andreev oscillations induced by step-like spin–orbit coupling, *Phys. Rev. Lett.* 122(14), 147701 (2019)
24. R. Chen, T. Liu, C. M. Wang, H. Z. Lu, and X. C. Xie, Field tunable one sided higher-order topological hinge states in Dirac semimetals, *Phys. Rev. Lett.* 127(6), 066801 (2021)
25. R. Chen, C. M. Wang, T. Liu, H. Z. Lu, and X. C. Xie, Quantum Hall effect originated from helical edge states in Cd_3As_2, *Phys. Rev. Res.* 3(3), 033227 (2021)
26. B. Wan, F. Schindler, K. Wang, K. Wu, X. Wan, T. Neupert, and H. Z. Lu, Theory for the negative longitudinal magnetoresistance in the quantum limit of Kramers Weyl semimetals, *J. Phys.: Condens. Matter* 30(50), 505501 (2018)
27. C. L. Zhang, et al., Nonsaturating quantum magnetization in Weyl semimetal TaAs, *Nat. Commun.* 10, 1028 (2019)
28. F. Qin, S. Li, Z. Z. Du, C. M. Wang, W. Zhang, D. Yu, H. Z. Lu, and X. C. Xie, Theory for the charge density wave mechanism of 3D quantum Hall effect, *Phys. Rev. Lett.* 125(20), 206601 (2020)
29. P. L. Zhao, H. Z. Lu, and X. C. Xie, Theory for magnetic field driven 3D metal–insulator transitions in the quantum limit, *Phys. Rev. Lett.* 127(4), 046602 (2021)
30. S. Q. Shen, Topological Insulators, 2nd Ed., Springer Verlag, Berlin Heidelberg, 2017
31. R. Okugawa and S. Murakami, Dispersion of Fermi arcs in Weyl semimetals and their evolutions to Dirac cones, *Phys. Rev. B* 89(23), 235315 (2014)
32. H. Z. Lu, S. B. Zhang, and S. Q. Shen, High field mag netoconductivity of topological semimetals with short range potential, *Phys. Rev. B* 92(4), 045203 (2015)
33. H. Zheng and M. Zahid Hasan, Quasiparticle interference on type I and type II Weyl semimetal surfaces: A review, *Adv. Phys. X* 3(1), 1466661 (2018)
34. H. Z. Lu, W. Y. Shan, W. Yao, Q. Niu, and S. Q. Shen, Massive Dirac fermions and spin physics in an ultrathin film of topological insulator, *Phys. Rev. B* 81(11), 115407 (2010)
35. C. M. Wang and X. L. Lei, Linear magnetoresistance on the topological surface, *Phys. Rev. B* 86(3), 035442 (2012)
36. Z. Wang, H. Weng, Q. Wu, X. Dai, and Z. Fang, Three-dimensional Dirac semimetal and quantum transport in Cd_3As_2, *Phys. Rev. B* 88(12), 125427 (2013)
37. S. Jeon, B. B. Zhou, A. Gyenis, B. E. Feldman, I. Kimchi, A. C. Potter, Q. D. Gibson, R. J. Cava, A. Vishwanath, and A. Yazdani, Landau quantization and quasiparticle interference in the three-dimensional

Dirac semimetal Cd_3As_2, *Nat. Mater.* 13(9), 851 (2014)
38. C. L. Zhang, F. Schindler, H. Liu, T. R. Chang, S. Y. Xu, G. Chang, W. Hua, H. Jiang, Z. Yuan, J. Sun, H. T. Jeng, H. Z. Lu, H. Lin, M. Z. Hasan, X. C. Xie, T. Neupert, and S. Jia, Ultraquantum magnetoresistance in the Kramers–Weyl semimetal candidate β-Ag_2Se, *Phys. Rev. B* 96(16), 165148 (2017)
39. E. H. Hall, et al., On a new action of the magnet on electric currents, *Am. J. Math.* 2(3), 287 (1879)
40. E. H. Hall, Xviii. on the "rotational coefficient" in nickel and cobalt, *Lond. Edinb. Dublin Philos. Mag. J. Sci.* 12(74), 157 (1881)
41. K. Klitzing, G. Dorda, and M. Pepper, New method for high accuracy determination of the fine structure constant based on quantized Hall resistance, *Phys. Rev. Lett.* 45(6), 494 (1980)
42. D. C. Tsui, H. L. Stormer, and A. C. Gossard, Two dimensional magnetotransport in the extreme quantum limit, *Phys. Rev. Lett.* 48(22), 1559 (1982)
43. N. Nagaosa, J. Sinova, S. Onoda, A. H. MacDonald, and N. P. Ong, Anomalous Hall effect, *Rev. Mod. Phys.* 82(2), 1539 (2010)
44. M. E. Cage, K. Klitzing, A. Chang, F. Duncan, M. Haldane, R. B. Laughlin, A. Pruisken, and D. Thouless, The Quantum Hall Effect, Springer Science & Business Media, 2012
45. I. Sodemann and L. Fu, Quantum nonlinear Hall effect induced by Berry curvature dipole in time reversal in variant materials, *Phys. Rev. Lett.* 115(21), 216806 (2015)
46. T. Low, Y. Jiang, and F. Guinea, Topological currents in black phosphorus with broken inversion symmetry, *Phys. Rev. B* 92(23), 235447 (2015)
47. J. I. Facio, D. Efremov, K. Koepernik, J. S. You, I. Sodemann, and J. van den Brink, Strongly enhanced berry dipole at topological phase transitions in BiTeI, *Phys. Rev. Lett.* 121(24), 246403 (2018)
48. J. S. You, S. Fang, S. Y. Xu, E. Kaxiras, and T. Low, Berry curvature dipole current in the transition metal dichalcogenides family, *Phys. Rev. B* 98(12), 121109 (2018)
49. Y. Zhang, J. van den Brink, C. Felser, and B. Yan, Electrically tuneable nonlinear anomalous Hall effect in two-dimensional transition metal dichalcogenides WTe_2 and $MoTe_2$, *2D Mater.* 5, 044001 (2018)
50. Y. Zhang, Y. Sun, and B. Yan, Berry curvature dipole in Weyl semimetal materials: An *ab initio* study, *Phys. Rev. B* 97(4), 041101 (2018)
51. M. Papaj and L. Fu, Magnus Hall effect, *Phys. Rev. Lett.* 123(21), 216802 (2019)
52. D. Mandal, K. Das, and A. Agarwal, Magnus Nernst and thermal Hall effect, *Phys. Rev. B* 102(20), 205414 (2020)
53. K. Hamamoto, M. Ezawa, K. W. Kim, T. Morimoto, and N. Nagaosa, Nonlinear spin current generation in noncentrosymmetric spin–orbit coupled systems, *Phys. Rev. B* 95(22), 224430 (2017)
54. Y. Araki, Strain-induced nonlinear spin Hall effect in topological Dirac semimetal, *Sci. Rep.* 8(1), 15236 (2018)
55. X. Q. Yu, Z. G. Zhu, J. S. You, T. Low, and G. Su, Topological nonlinear anomalous nernst effect in strained transition metal dichalcogenides, *Phys. Rev. B* 99(20), 201410 (2019)
56. C. Zeng, S. Nandy, A. Taraphder, and S. Tewari, Nonlinear Nernst effect in bilayer WTe_2, *Phys. Rev. B* 100(24), 245102 (2019)
57. R. Nakai and N. Nagaosa, Nonreciprocal thermal and thermoelectric transport of electrons in noncentrosymmetric crystals, *Phys. Rev. B* 99(11), 115201 (2019)
58. C. Zeng, S. Nandy, and S. Tewari, Fundamental relations for anomalous thermoelectric transport coefficients in the nonlinear regime, *Phys. Rev. Res.* 2(3), 032066 (2020)
59. K. Kang, T. Li, E. Sohn, J. Shan, and K. F. Mak, Nonlinear anomalous Hall effect in few layer WTe_2, *Nat. Mater.* 18(4), 324 (2019)
60. M. V. Berry, Quantal phase factors accompanying adiabatic changes, *Proc. R. Soc. Lond. A* 392(1802), 45 (1984)
61. D. Xiao, M. C. Chang, and Q. Niu, Berry phase effects on electronic properties, *Rev. Mod. Phys.* 82(3), 1959 (2010)
62. R. Karplus and J. M. Luttinger, Hall effect in ferromagnetics, *Phys. Rev.* 95(5), 1154 (1954)
63. W. A. Benalcazar, B. A. Bernevig, and T. L. Hughes, Quantized electric multipole insulators, *Science* 357(6346), 61 (2017)
64. W. A. Benalcazar, B. A. Bernevig, and T. L. Hughes, Electric multipole moments, topological multipole moment pumping, and chiral hinge states in crystalline insulators, *Phys. Rev. B* 96(24), 245115 (2017)
65. C. M. Wang, H. P. Sun, H. Z. Lu, and X. C. Xie, 3D quantum Hall effect of Fermi arcs in topological semimetals, *Phys. Rev. Lett.* 119(13), 136806 (2017)
66. Z. Song, Z. Fang, and C. Fang, $(d-2)$ dimensional edge states of rotation symmetry protected topological states, *Phys. Rev. Lett.* 119(24), 246402 (2017)
67. J. Langbehn, Y. Peng, L. Trifunovic, F. von Oppen, and P. W. Brouwer, Reflection symmetric second-order topological insulators and superconductors, *Phys. Rev. Lett.* 119(24), 246401 (2017)
68. R. Chen, C. Z. Chen, J. H. Gao, B. Zhou, and D. H. Xu, Higher-order topological insulators in quasicrystals, *Phys. Rev. Lett.* 124(3), 036803 (2020)
69. F. Schindler, A. M. Cook, M. G. Vergniory, Z. Wang, S. S. P. Parkin, B. A. Bernevig, and T. Neupert, Higher-order topological insulators, *Sci. Adv.* 4(6), eaat0346 (2018)
70. F. Schindler, Z. Wang, M. G. Vergniory, A. M. Cook, A. Murani, S. Sengupta, A. Y. Kasumov, R. Deblock, S. Jeon, I. Drozdov, H. Bouchiat, S. Guéron, A. Yazdani, B. A. Bernevig, and T. Neupert, Higher-order topology in bismuth, *Nat. Phys.* 14(9), 918 (2018)
71. M. Ezawa, Higher-order topological insulators and semimetals on the breathing Kagome and pyrochlore lattices, *Phys. Rev. Lett.* 120(2), 026801 (2018)
72. Z. Li, Y. Cao, P. Yan, and X. Wang, Higher-order topological solitonic insulators, *npj Comput. Mater.* 5, 107 (2019)
73. L. Fu, C. L. Kane, and E. J. Mele, Topological insulators in three dimensions, *Phys. Rev. Lett.* 98(10), 106803

(2007)
74. J. E. Moore and L. Balents, Topological invariants of time reversal invariant band structures, *Phys. Rev. B* 75(12), 121306 (2007)
75. S. Murakami, Phase transition between the quantum spin Hall and insulator phases in 3D: Emergence of a topological gapless phase, *New J. Phys.* 9(9), 356 (2007)
76. R. Roy, Topological phases and the quantum spin Hall effect in three dimensions, *Phys. Rev. B* 79(19), 195322 (2009)
77. L. Fu and C. L. Kane, Topological insulators within version symmetry, *Phys. Rev. B* 76(4), 045302 (2007)
78. D. Hsieh, D. Qian, L. Wray, Y. Xia, Y. S. Hor, R. J. Cava, and M. Z. Hasan, A topological Dirac insulator in a quantum spin Hall phase, *Nature* 452(7190), 970 (2008)
79. H. Zhang, C. X. Liu, X. L. Qi, X. Dai, Z. Fang, and S. C. Zhang, Topological insulators in Bi_2Se_3, Bi_2Te_3 and Sb_2Te_3 with a single Dirac cone on the surface, *Nat. Phys.* 5(6), 438 (2009)
80. Y. Xia, D. Qian, D. Hsieh, L. Wray, A. Pal, H. Lin, A. Bansil, D. Grauer, Y. S. Hor, R. J. Cava, and M. Z. Hasan, Observation of a large gap topological insulator class with a single Dirac cone on the surface, *Nat. Phys.* 5(6), 398 (2009)
81. M. Z. Hasan and C. L. Kane, Colloquium: Topological insulators, *Rev. Mod. Phys.* 82(4), 3045 (2010)
82. X. L. Qi and S. C. Zhang, Topological insulators and superconductors, *Rev. Mod. Phys.* 83(4), 1057 (2011)
83. M. Z. Hasan and J. E. Moore, Three-dimensional topological insulators, *Annu. Rev. Condens. Matter Phys.* 2(1), 55 (2011)
84. H. Xue, Y. Yang, F. Gao, Y. Chong, and B. Zhang, Acoustic higher-order topological insulator on a Kagome lattice, *Nat. Mater.* 18(2), 108 (2019)
85. X. Ni, M. Weiner, A. Alù, and A. B. Khanikaev, Observation of higher-order topological acoustic states protected by generalized chiral symmetry, *Nat. Mater.* 18(2), 113 (2019)
86. H. Xue, Y. Ge, H. X. Sun, Q. Wang, D. Jia, Y. J. Guan, S. Q. Yuan, Y. Chong, and B. Zhang, Observation of an acoustic octupole topological insulator, *Nat. Commun.* 11(1), 2442 (2020)
87. M. Serra-Garcia, V. Peri, R. Süsstrunk, O. R. Bilal, T. Larsen, L. G. Villanueva, and S. D. Huber, Observation of a phononic quadrupole topological insulator, *Nature* 555(7696), 342 (2018)
88. C. W. Peterson, W. A. Benalcazar, T. L. Hughes, and G. Bahl, A quantized microwave quadrupole insulator with topologically protected corner states, *Nature* 555(7696), 346 (2018)
89. S. Imhof, C. Berger, F. Bayer, J. Brehm, L. W. Molenkamp, T. Kiessling, F. Schindler, C. H. Lee, M. Greiter, T. Neupert, and R. Thomale, Topoelectrical circuit realization of topological corner modes, *Nat. Phys.* 14(9), 925 (2018)
90. M. Serra-Garcia, R. Süsstrunk, and S. D. Huber, Observation of quadrupole transitions and edge mode topology in an LC circuit network, *Phys. Rev. B* 99, 020304(R) (2019)
91. S. Mittal, V. V. Orre, G. Zhu, M. A. Gorlach, A. Poddubny, and M. Hafezi, Photonic quadrupole topological phases, *Nat. Photonics* 13(10), 692 (2019)
92. A. El Hassan, F. K. Kunst, A. Moritz, G. Andler, E. J. Bergholtz, and M. Bourennane, Corner states of light in photonic waveguides, *Nat. Photonics* 13(10), 697 (2019)
93. B. Y. Xie, G. X. Su, H. F. Wang, H. Su, X. P. Shen, P. Zhan, M. H. Lu, Z. L. Wang, and Y. F. Chen, Visualization of higher-order topological insulating phases in two-dimensional dielectric photonic crystals, *Phys. Rev. Lett.* 122(23), 233903 (2019)
94. M. Li, D. Zhirihin, M. Gorlach, X. Ni, D. Filonov, A. Slobozhanyuk, A. Alù, and A. B. Khanikaev, Higher-order topological states in photonic Kagome crystals with long range interactions, *Nat. Photonics* 14(2), 89 (2020)
95. Y. Xu, Z. Song, Z. Wang, H. Weng, and X. Dai, Higher-order topology of the axion insula tor $EuIn_2As_2$, *Phys. Rev. Lett.* 122(25), 256402 (2019)
96. R. X. Zhang, F. Wu, and S. Das Sarma, Möbius insulator and higher-order topology in $MnBi_{2n}Te_{3n+1}$, *Phys. Rev. Lett.* 124(13), 136407 (2020)
97. J. E. Moore, The birth of topological insulators, *Nature* 464(7286), 194 (2010)
98. Z. Zhu, M. Papaj, X. A. Nie, H. K. Xu, Y. S. Gu, X. Yang, D. Guan, S. Wang, Y. Li, C. Liu, J. Luo, Z. A. Xu, H. Zheng, L. Fu, and J. F. Jia, Discovery of segmented Fermi surface induced by cooper pair momentum, *Science* 374(6573), 1381 (2021)
99. C. X. Liu, X. L. Qi, X. Dai, Z. Fang, and S. C. Zhang, Quantum anomalous Hall effect in $Hg_{1-y}Mn_yTe$ quantum wells, *Phys. Rev. Lett.* 101(14), 146802 (2008)
100. R. Yu, W. Zhang, H. J. Zhang, S. C. Zhang, X. Dai, and Z. Fang, Quantized anomalous Hall effect in magnetic topological insulators, *Science* 329(5987), 61 (2010)
101. X. A. Nie, S. Li, M. Yang, Z. Zhu, H. K. Xu, X. Yang, F. Zheng, D. Guan, S. Wang, Y. Y. Li, C. Liu, J. Li, P. Zhang, Y. Shi, H. Zheng, and J. Jia, Robust hot electron and multiple topological insulator states in $PtBi_2$, *ACS Nano* 14(2), 2366 (2020)
102. Z. Zhu, T. R. Chang, C. Y. Huang, H. Pan, X. A. Nie, X. Z. Wang, Z. T. Jin, S. Y. Xu, S. M. Huang, D. D. Guan, S. Wang, Y. Y. Li, C. Liu, D. Qian, W. Ku, F. Song, H. Lin, H. Zheng, and J. F. Jia, Quasiparticle interference and nonsymmorphic effect on a floating band surface state of zrsise, *Nat. Commun.* 9(1), 4153 (2018)
103. M. Mogi, R. Yoshimi, A. Tsukazaki, K. Yasuda, Y. Kozuka, K. Takahashi, M. Kawasaki, and Y. Tokura, Magnetic modulation doping in topological insulators toward higher temperature quantum anomalous Hall effect, *Appl. Phys. Lett.* 107(18), 182401 (2015)
104. Y. Tokura, K. Yasuda, and A. Tsukazaki, Magnetic topological insulators, *Nat. Rev. Phys.* 1(2), 126 (2019)
105. M. M. Otrokov, I. I. Klimovskikh, H. Bentmann, D. Estyunin, A. Zeugner, Z. S. Aliev, S. Gaß, A. U. B. Wolter, A. V. Koroleva, A. M. Shikin, M. Blanco-Rey, M. Hoffmann, I. P. Rusinov, A. Y. Vyazovskaya, S. V. Eremeev, Y. M. Koroteev, V. M. Kuznetsov, F. Freyse,

J. Sánchez-Barriga, I. R. Amiraslanov, M. B. Babanly, N. T. Mamedov, N. A. Abdullayev, V. N. Zverev, A. Alfonsov, V. Kataev, B. Büchner, E. F. Schwier, S. Kumar, A. Kimura, L. Petaccia, G. Di Santo, R. C. Vidal, S. Schatz, K. Kißner, M. Ünzelmann, C. H. Min, S. Moser, T. R. F. Peixoto, F. Reinert, A. Ernst, P. M. Echenique, A. Isaeva, and E. V. Chulkov, Prediction and observation of an antiferromagnetic topological insulator, *Nature* 576(7787), 416 (2019)

106. D. Zhang, M. Shi, T. Zhu, D. Xing, H. Zhang, and J. Wang, Topological axion states in the magnetic insulator $MnBi_2Te_4$ with the quantized magnetoelectric effect, *Phys. Rev. Lett.* 122(20), 206401 (2019)
107. J. Li, Y. Li, S. Du, Z. Wang, B. L. Gu, S. C. Zhang, K. He, W. Duan, and Y. Xu, Intrinsic magnetic topological insulators in van der Waals layered $MnBi_2Te_4$ family materials, *Sci. Adv.* 5(6), eaaw5685 (2019)
108. H. K. Xu, M. Gu, F. Fei, Y. S. Gu, D. Liu, Q. Y. Yu, S. S. Xue, X. H. Ning, B. Chen, H. Xie, Z. Zhu, D. Guan, S. Wang, Y. Li, C. Liu, Q. Liu, F. Song, H. Zheng, and J. Jia, Observation of magnetism-induced topological edge state in antiferromagnetic topological insulator $MnBi_4Te_7$, *ACS Nano* 16(6), 9810 (2022)
109. Y. J. Hao, P. Liu, Y. Feng, X. M. Ma, E. F. Schwier, M. Arita, S. Kumar, C. Hu, R. Lu, M. Zeng, Y. Wang, Z. Hao, H. Y. Sun, K. Zhang, J. Mei, N. Ni, L. Wu, K. Shimada, C. Chen, Q. Liu, and C. Liu, Gapless surface Dirac cone in antiferromagnetic topological insulator $MnBi_2Te_4$, *Phys. Rev. X* 9(4), 041038 (2019)
110. Y. J. Chen, L. X. Xu, J. H. Li, Y. W. Li, H. Y. Wang, C. F. Zhang, H. Li, Y. Wu, A. J. Liang, C. Chen, S. W. Jung, C. Cacho, Y. H. Mao, S. Liu, M. X. Wang, Y. F. Guo, Y. Xu, Z. K. Liu, L. X. Yang, and Y. L. Chen, Topological electronic structure and its temperature evolution in antiferromagnetic topological insulator $MnBi_2Te_4$, *Phys. Rev. X* 9(4), 041040 (2019)
111. P. Swatek, Y. Wu, L. L. Wang, K. Lee, B. Schrunk, J. Yan, and A. Kaminski, Gapless Dirac surface states in the antiferromagnetic topological insulator $MnBi_2Te_4$, *Phys. Rev. B* 101(16), 161109 (2020)
112. R. D. Peccei and H. R. Quinn, CP conservation in the presence of pseudoparticles, *Phys. Rev. Lett.* 38(25), 1440 (1977)
113. J. Wang, B. Lian, X. L. Qi, and S. C. Zhang, Quantized topological magnetoelectric effect of the zero plateau quantum anomalous Hall state, *Phys. Rev. B* 92(8), 081107 (2015)
114. T. Morimoto, A. Furusaki, and N. Nagaosa, Topological magnetoelectric effects in thin films of topological insulators, *Phys. Rev. B* 92(8), 085113 (2015)
115. X. L. Qi, R. Li, J. Zang, and S. C. Zhang, Inducing a magnetic monopole with topological surface states, *Science* 323(5918), 1184 (2009)
116. J. Maciejko, X. L. Qi, H. D. Drew, and S. C. Zhang, Topological quantization in units of the fine structure constant, *Phys. Rev. Lett.* 105(16), 166803 (2010)
117. W. K. Tse and A. H. MacDonald, Giant magneto optical Kerr effect and universal faraday effect in thin film topological insulators, *Phys. Rev. Lett.* 105(5), 057401 (2010)
118. J. Yu, J. Zang, and C. X. Liu, Magnetic resonance induced pseudoelectric field and giant current response in axion insulators, *Phys. Rev. B* 100(7), 075303 (2019)
119. R. Chen, H. P. Sun, and B. Zhou, Side surface mediated hybridization in axion insulators, *Phys. Rev. B* 107(12), 125304 (2023)
120. A. M. Essin, J. E. Moore, and D. Vanderbilt, Magnetoelectric polarizability and axion electrodynamics in crystalline insulators, *Phys. Rev. Lett.* 102(14), 146805 (2009)
121. R. S. K. Mong, A. M. Essin, and J. E. Moore, Anti ferromagnetic topological insulators, *Phys. Rev. B* 81(24), 245209 (2010)
122. C. Niu, H. Wang, N. Mao, B. Huang, Y. Mokrousov, and Y. Dai, Antiferromagnetic topological insulator with nonsymmorphic protection in two dimensions, *Phys. Rev. Lett.* 124(6), 066401 (2020)
123. Y. Xu, I. Miotkowski, C. Liu, J. Tian, H. Nam, N. Alidoust, J. Hu, C. K. Shih, M. Z. Hasan, and Y. P. Chen, Observation of topological surface state quantum Hall effect in an intrinsic three-dimensional topological insulator, *Nat. Phys.* 10(12), 956 (2014)
124. A. MacKinnon, The calculation of transport properties and density of states of disordered solids, *Z. Phys. B* 59(4), 385 (1985)
125. G. Metalidis and P. Bruno, Green's function technique for studying electron flow in two-dimensional mesoscopic samples, *Phys. Rev. B* 72(23), 235304 (2005)
126. R. Landauer, Electrical resistance of disordered one dimensional lattices, *Philosophical Magazine* 21, 863 (1970)
127. M. Büttiker, Absence of backscattering in the quantum Hall effect in multiprobe conductors, *Phys. Rev. B* 38(14), 9375 (1988)
128. D. S. Fisher and P. A. Lee, Relation between conductivity and transmission matrix, *Phys. Rev. B* 23(12), 6851 (1981)
129. R. L. Chu, J. Shi, and S. Q. Shen, Surface edge state and half quantized Hall conductance in topological insulators, *Phys. Rev. B* 84(8), 085312 (2011)
130. J. Alicea, New directions in the pursuit of Majorana fermions in solid state systems, *Rep. Prog. Phys.* 75(7), 076501 (2012)
131. M. Leijnse and K. Flensberg, Introduction to topological superconductivity and Majorana fermions, *Semicond. Sci. Technol.* 27(12), 124003 (2012)
132. C. Beenakker, Search for Majorana fermions in superconductors, *Annu. Rev. Condens. Matter Phys.* 4(1), 113 (2013)
133. T. D. Stanescu and S. Tewari, Majorana fermions in semiconductor nanowires: Fundamentals, modeling, and experiment, *J. Phys.: Condens. Matter* 25(23), 233201 (2013)
134. R. Aguado, Majorana quasiparticles in condensed matter, *Riv. Nuovo Cim.* 40, 523 (2017)
135. A. Kitaev, Fault-tolerant quantum computation by anyons, *Ann. Phys.* 303(1), 2 (2003)
136. C. Nayak, S. H. Simon, A. Stern, M. Freedman, and S. Das Sarma, Nonabelian anyons and topological quantum computation, *Rev. Mod. Phys.* 80(3), 1083 (2008)
137. S. D. Sarma, M. Freedman, and C. Nayak, Majorana zero modes and topological quantum computation, *npj*

Quantum Inf. 1, 15001 (2015)
138. V. Mourik, K. Zuo, S. M. Frolov, S. R. Plissard, E. P. A. M. Bakkers, and L. P. Kouwenhoven, Signatures of Majorana fermions in hybrid superconductor semiconductor nanowire devices, *Science* 336(6084), 1003 (2012)
139. M. Deng, C. Yu, G. Huang, M. Larsson, P. Caroff, and H. Xu, Anomalous zerobias conductance peak in a NbInSb nanowire–Nb hybrid device, *Nano Lett.* 12(12), 6414 (2012)
140. A. Das, Y. Ronen, Y. Most, Y. Oreg, M. Heiblum, and H. Shtrikman, Zero bias peaks and splitting in an AlInAs nanowire topological superconductor as a signature of Majorana fermions, *Nat. Phys.* 8(12), 887 (2012)
141. A. D. K. Finck, D. J. Van Harlingen, P. K. Mohseni, K. Jung, and X. Li, Anomalous modulation of a zero bias peak in a hybrid nanowire superconductor device, *Phys. Rev. Lett.* 110(12), 126406 (2013)
142. H. O. H. Churchill, V. Fatemi, K. Grove-Rasmussen, M. T. Deng, P. Caroff, H. Q. Xu, and C. M. Marcus, Superconductor-nanowire devices from tunneling to the multichannel regime: Zero-bias oscillations and magnetoconductance crossover, *Phys. Rev. B* 87(24), 241401 (2013)
143. M. T. Deng, S. Vaitieke˙nas, E. B. Hansen, J. Danon, M. Leijnse, K. Flensberg, J. Nygård, P. Krogstrup, and C. M. Marcus, Majorana bound state in a coupled quantum dot hybrid nanowire system, *Science* 354(6319), 1557 (2016)
144. J. Chen, P. Yu, J. Stenger, M. Hocevar, D. Car, S. R. Plissard, E. P. A. M. Bakkers, T. D. Stanescu, and S. M. Frolov, Experimental phase diagram of zero bias conductance peaks in superconductor/semiconductor nanowire devices, *Sci. Adv.* 3(9), e1701476 (2017)
145. H. J. Suominen, M. Kjaergaard, A. R. Hamilton, J. Shabani, C. J. Palmstrøm, C. M. Marcus, and F. Nichele, Zero energy modes from coalescing Andreev states in a two-dimensional semiconductor–superconductor hybrid platform, *Phys. Rev. Lett.* 119(17), 176805 (2017)
146. F. Nichele, A. C. C. Drachmann, A. M. Whiticar, E. C. T. O'Farrell, H. J. Suominen, A. Fornieri, T. Wang, G. C. Gardner, C. Thomas, A. T. Hatke, P. Krogstrup, M. J. Manfra, K. Flensberg, and C. M. Marcus, Scaling of Majorana zero bias conductance peaks, *Phys. Rev. Lett.* 119(13), 136803 (2017)
147. H. Zhang, C. X. Liu, S. Gazibegovic, D. Xu, J. A. Logan, G. Wang, N. van Loo, J. D. S. Bommer, M. W. A. de Moor, D. Car, R. L. M. Op het Veld, P. J. van Veldhoven, S. Koelling, M. A. Verheijen, M. Pendharkar, D. J. Pennachio, B. Shojaei, J. S. Lee, C. J. Palmstrøm, E. P. A. M. Bakkers, S. D. Sarma, and L. P. Kouwenhoven, Retracted article: Quantized Majorana conductance, *Nature* 556(7699), 74 (2018)
148. J. E. Sestoft, T. Kanne, A. N. Gejl, M. von Soosten, J. S. Yodh, D. Sherman, B. Tarasinski, M. Wimmer, E. Johnson, M. Deng, J. Nygård, T. S. Jespersen, C. M. Marcus, and P. Krogstrup, Engineering hybrid epitaxial InAsSb/Al nanowires for stronger topological protection, *Phys. Rev. Mater.* 2(4), 044202 (2018)
149. S. Vaitiekėnas, M. T. Deng, J. Nygård, P. Krogstrup, and C. M. Marcus, Effective g factor of subgap states in hybrid nanowires, *Phys. Rev. Lett.* 121(3), 037703 (2018)
150. M. T. Deng, S. Vaitieke˙nas, E. Prada, P. SanJose, J. Nygård, P. Krogstrup, R. Aguado, and C. M. Marcus, Nonlocality of Majorana modes in hybrid nanowires, *Phys. Rev. B* 98(8), 085125 (2018)
151. M. W. A. de Moor, J. D. S. Bommer, D. Xu, G. W. Winkler, A. E. Antipov, A. Bargerbos, G. Wang, N. Loo, R. L. M. Op het Veld, S. Gazibegovic, D. Car, J. A. Logan, M. Pendharkar, J. S. Lee, E. P. A. M Bakkers, C. J. Palmstrøm, R. M. Lutchyn, L. P. Kouwenhoven, and H. Zhang, Electric field tunable superconductor semiconductor coupling in Majorana nanowires, *New J. Phys.* 20(10), 103049 (2018)
152. Z. Zhu, H. Zheng, and J. F. Jia, Majorana zero mode in the vortex of artificial topological superconductor, *J. Appl. Phys.* 129(15), 151104 (2021)
153. R. M. Lutchyn, J. D. Sau, and S. Das Sarma, Majorana fermions and a topological phase transition in semiconductor-superconductor heterostructures, *Phys. Rev. Lett.* 105(7), 077001 (2010)
154. Y. Oreg, G. Refael, and F. von Oppen, Helical liquids and Majorana bound states in quantum wires, *Phys. Rev. Lett.* 105(17), 177002 (2010)
155. R. M. Lutchyn, E. P. Bakkers, L. P. Kouwenhoven, P. Krogstrup, C. M. Marcus, and Y. Oreg, Majorana zero modes in superconductor–semiconductor heterostructures, *Nat. Rev. Mater.* 3(5), 52 (2018)
156. E. Prada, P. San-Jose, and R. Aguado, Transport spectroscopy of *NS* nanowire junctions with Majorana fermions, *Phys. Rev. B* 86(18), 180503 (2012)
157. S. Das Sarma, J. D. Sau, and T. D. Stanescu, Splitting of the zero bias conductance peak as smoking gun evidence for the existence of the Majorana mode in a superconductor–semiconductor nanowire, *Phys. Rev. B* 86(22), 220506 (2012)
158. D. Rainis, L. Trifunovic, J. Klinovaja, and D. Loss, Towards a realistic transport modeling in a superconducting nanowire with majorana fermions, *Phys. Rev. B* 87(2), 024515 (2013)
159. S. M. Albrecht, A. P. Higginbotham, M. Madsen, F. Kuemmeth, T. S. Jespersen, J. Nygård, P. Krogstrup, and C. Marcus, Exponential protection of zero modes in Majorana islands, *Nature* 531(7593), 206 (2016)
160. D. Sherman, J. Yodh, S. Albrecht, J. Nygård, P. Krogstrup, and C. Marcus, Normal, superconducting and topological regimes of hybrid double quantum dots, *Nat. Nanotechnol.* 12(3), 212 (2017)
161. S. M. Albrecht, E. B. Hansen, A. P. Higginbotham, F. Kuemmeth, T. S. Jespersen, J. Nygård, P. Krogstrup, J. Danon, K. Flensberg, and C. M. Marcus, Transport signatures of quasiparticle poisoning in a Majorana island, *Phys. Rev. Lett.* 118(13), 137701 (2017)
162. E. C. T. O'Farrell, A. C. C. Drachmann, M. Hell, A. Fornieri, A. M. Whiticar, E. B. Hansen, S. Gronin, G. C. Gardner, C. Thomas, M. J. Manfra, K. Flensberg, C. M. Marcus, and F. Nichele, Hybridization of subgap states in one-dimensional superconductor semiconductor Coulomb islands, *Phys. Rev. Lett.* 121(25), 256803

(2018)
163. G. Kells, D. Meidan, and P. W. Brouwer, Nearzero energy end states in topologically trivial spin–orbit coupled superconducting nanowires with a smooth confinement, *Phys. Rev. B* 86(10), 100503 (2012)
164. T. D. Stanescu and S. Tewari, Disentangling Majorana fermions from topologically trivial low energy states in semiconductor Majorana wires, *Phys. Rev. B* 87(14), 140504 (2013)
165. C. X. Liu, J. D. Sau, T. D. Stanescu, and S. Das Sarma, Andreev bound states versus Majorana bound states in quantum dot nanowire superconductor hybrid structures: Trivial versus topological zero bias conductance peaks, *Phys. Rev. B* 96(7), 075161 (2017)
166. C. Moore, T. D. Stanescu, and S. Tewari, Two terminal charge tunneling: Disentangling Majorana zero modes from partially separated Andreev bound states in semiconductor–superconductor heterostructures, *Phys. Rev. B* 97(16), 165302 (2018)
167. B. I. Halperin, Possible states for a three-dimensional electron gas in a strong magnetic field, *Jpn. J. Appl. Phys.* 26(S3-3), 1913 (1987)
168. O. Zilberberg, S. Huang, J. Guglielmon, M. Wang, K. P. Chen, Y. E. Kraus, and M. C. Rechtsman, Photonic topological boundary pumping as a probe of 4D quantum Hall physics, *Nature* 553(7686), 59 (2018)
169. G. Montambaux and M. Kohmoto, Quantized Hall effect in three dimensions, *Phys. Rev. B* 41(16), 11417 (1990)
170. M. Kohmoto, B. I. Halperin, and Y. S. Wu, Diophan tine equation for the three-dimensional quantum Hall effect, *Phys. Rev. B* 45(23), 13488 (1992)
171. M. Koshino, H. Aoki, K. Kuroki, S. Kagoshima, and T. Osada, Hofstadter butterfly and integer quantum Hall effect in three dimensions, *Phys. Rev. Lett.* 86(6), 1062 (2001)
172. B. A. Bernevig, T. L. Hughes, S. Raghu, and D. P. Arovas, Theory of the three-dimensional quantum Hall effect in graphite, *Phys. Rev. Lett.* 99(14), 146804 (2007)
173. H. L. Störmer, J. P. Eisenstein, A. C. Gossard, W. Wiegmann, and K. Baldwin, Quantization of the Hall effect in an anisotropic three-dimensional electronic system, *Phys. Rev. Lett.* 56(1), 85 (1986)
174. J. R. Cooper, W. Kang, P. Auban, G. Montambaux, D. Jérome, and K. Bechgaard, Quantized Hall effect and a new field-induced phase transition in the organic superconductor $(TMTSF)_2PF_6$, *Phys. Rev. Lett.* 63(18), 1984 (1989)
175. S. T. Hannahs, J. S. Brooks, W. Kang, L. Y. Chiang, and P. M. Chaikin, Quantum Hall effect in a bulk crystal, *Phys. Rev. Lett.* 63(18), 1988 (1989)
176. S. Hill, S. Uji, M. Takashita, C. Terakura, T. Terashima, H. Aoki, J. S. Brooks, Z. Fisk, and J. Sarrao, Bulk quantum Hall effect in η-Mo_4O_{11}, *Phys. Rev. B* 58(16), 10778 (1998)
177. H. Cao, J. Tian, I. Miotkowski, T. Shen, J. Hu, S. Qiao, and Y. P. Chen, Quantized Hall effect and Shubnikov–de Haas oscillations in highly doped Bi_2Se_3: Evidence for layered transport of bulk carriers, *Phys. Rev. Lett.* 108(21), 216803 (2012)
178. H. Masuda, H. Sakai, M. Tokunaga, Y. Yamasaki, A. Miyake, J. Shiogai, S. Nakamura, S. Awaji, A. Tsukazaki, H. Nakao, Y. Murakami, T. Arima, Y. Tokura, and S. Ishiwata, Quantum Hall effect in a bulk antiferromagnet $EuMnBi_2$ with magnetically confined two-dimensional Dirac fermions, *Sci. Adv.* 2(1), e1501117 (2016)
179. Y. Liu, X. Yuan, C. Zhang, Z. Jin, A. Narayan, C. Luo, Z. Chen, L. Yang, J. Zou, X. Wu, S. Sanvito, Z. Xia, L. Li, Z. Wang, and F. Xiu, Zeeman splitting and dynamical mass generation in Dirac semimetal $ZrTe_5$, *Nat. Commun.* 7(1), 12516 (2016)
180. J. Liu, J. Yu, J. L. Ning, H. M. Yi, L. Miao, L. J. Min, Y. F. Zhao, W. Ning, K. A. Lopez, Y. L. Zhu, T. Pillsbury, Y. B. Zhang, Y. Wang, J. Hu, H. B. Cao, B. C. Chakoumakos, F. Balakirev, F. Weickert, M. Jaime, Y. Lai, K. Yang, J. W. Sun, N. Alem, V. Gopalan, C. Z. Chang, N. Samarth, C. X. Liu, R. D. McDonald, and Z. Q. Mao, Spin-valley locking and bulk quantum Hall effect in a noncentrosymmetric Dirac semimetal $BaMnSb_2$, *Nat. Commun.* 12(1), 4062 (2021)
181. F. Tang, Y. Ren, P. Wang, R. Zhong, J. Schneeloch, S. A. Yang, K. Yang, P. A. Lee, G. Gu, Z. Qiao, and L. Zhang, Three-dimensional quantum Hall effect and metal–insulator transition in $ZrTe_5$, *Nature* 569(7757), 537 (2019)
182. H. Li, H. Liu, H. Jiang, and X. C. Xie, 3D quantum Hall effect and a global picture of edge states in Weyl semimetals, *Phys. Rev. Lett.* 125(3), 036602 (2020)
183. S. G. Cheng, H. Jiang, Q. F. Sun, and X. C. Xie, Quantum Hall effect in wedge-shaped samples, *Phys. Rev. B* 102(7), 075304 (2020)
184. P. Wang, Y. Ren, F. Tang, P. Wang, T. Hou, H. Zeng, L. Zhang, and Z. Qiao, Approaching three-dimensional quantum Hall effect in bulk $HfTe_5$, *Phys. Rev. B* 101(16), 161201 (2020)
185. R. Ma, D. N. Sheng, and L. Sheng, Three-dimensional quantum Hall effect and magnetothermoelectric properties in Weyl semimetals, *Phys. Rev. B* 104(7), 075425 (2021)
186. S. C. Zhang and J. Hu, A four-dimensional generalization of the quantum Hall effect, *Science* 294(5543), 823 (2001)
187. M. Lohse, C. Schweizer, H. M. Price, O. Zilberberg, and I. Bloch, Exploring 4D quantum Hall physics with a 2D topological charge pump, *Nature* 553(7686), 55 (2018)
188. H. M. Price, O. Zilberberg, T. Ozawa, I. Carusotto, and N. Goldman, Four-dimensional quantum Hall effect with ultracold atoms, *Phys. Rev. Lett.* 115(19), 195303 (2015)
189. Y. J. Jin, R. Wang, B. W. Xia, B. B. Zheng, and H. Xu, Three-dimensional quantum anomalous Hall effect in ferromagnetic insulators, *Phys. Rev. B* 98(8), 081101 (2018)
190. R. A. Molina and J. González, Surface and 3D quantum Hall effects from engineering of exceptional points in nodal line semimetals, *Phys. Rev. Lett.* 120(14), 146601 (2018)
191. E. Benito-Matías, R. A. Molina, and J. González, Surface and bulk Landau levels in thin films of Weyl

semimetals, *Phys. Rev. B* 101(8), 085420 (2020)
192. M. Chang and L. Sheng, Three-dimensional quantum Hall effect in the excitonic phase of a Weyl semimetal, *Phys. Rev. B* 103(24), 245409 (2021)
193. M. Chang, H. Geng, L. Sheng, and D. Y. Xing, Three-dimensional quantum Hall effect in Weyl semimetals, *Phys. Rev. B* 103(24), 245434 (2021)
194. K. Klitzing, G. Dorda, and M. Pepper, New method for high accuracy determination of the fine structure constant based on quantized Hall resistance, *Phys. Rev. Lett.* 45(6), 494 (1980)
195. D. J. Thouless, M. Kohmoto, M. P. Nightingale, and M. den Nijs, Quantized Hall conductance in a two-dimensional periodic potential, *Phys. Rev. Lett.* 49(6), 405 (1982)
196. H. Z. Lu, 3D quantum Hall effect, *Natl. Sci. Rev.* 6(2), 208 (2019)
197. F. Liu, H. Y. Deng, and K. Wakabayashi, Helical topological edge states in a quadrupole phase, *Phys. Rev. Lett.* 122(8), 086804 (2019)
198. B. Roy, Antiunitary symmetry protected higher-order topological phases, *Phys. Rev. Res.* 1(3), 032048 (2019)
199. C. B. Hua, R. Chen, B. Zhou, and D. H. Xu, Higher-order topological insulator in a dodecagonal quasicrystal, *Phys. Rev. B* 102(24), 241102 (2020)
200. Z. R. Liu, L. H. Hu, C. Z. Chen, B. Zhou, and D. H. Xu, Topological excitonic corner states and nodal phase in bilayer quantum spin Hall insulators, *Phys. Rev. B* 103(20), L201115 (2021)
201. R. Queiroz and A. Stern, Splitting the hinge mode of higher-order topological insulators, *Phys. Rev. Lett.* 123(3), 036802 (2019)
202. M. Sitte, A. Rosch, E. Altman, and L. Fritz, Topological insulators in magnetic fields: Quantum Hall effect and edge channels with a nonquantized θ term, *Phys. Rev. Lett.* 108(12), 126807 (2012)
203. F. Zhang, C. L. Kane, and E. J. Mele, Surface state magnetization and chiral edge states on topological insulators, *Phys. Rev. Lett.* 110(4), 046404 (2013)
204. Y. Otaki and T. Fukui, Higher-order topological insulators in a magnetic field, *Phys. Rev. B* 100, 245108 (2019)
205. Z. Yan, F. Song, and Z. Wang, Majorana corner modes in a high temperature platform, *Phys. Rev. Lett.* 121(9), 096803 (2018)
206. Z. Yan, Higher-order topological odd parity superconductors, *Phys. Rev. Lett.* 123(17), 177001 (2019)
207. D. Varjas, A. Lau, K. Pöyhönen, A. R. Akhmerov, D. I. Pikulin, and I. C. Fulga, Topological phases without crystalline counterparts, *Phys. Rev. Lett.* 123(19), 196401 (2019)
208. S. A. A. Ghorashi, T. Li, and T. L. Hughes, Higher-order Weyl semimetals, *Phys. Rev. Lett.* 125(26), 266804 (2020)
209. H. X. Wang, Z. K. Lin, B. Jiang, G. Y. Guo, and J. H. Jiang, Higher-order weyl semimetals, *Phys. Rev. Lett.* 125(14), 146401 (2020)
210. K. Wang, J. X. Dai, L. B. Shao, S. A. Yang, and Y. X. Zhao, Boundary criticality of *PT* invariant topology and secondorder nodalline semimetals, *Phys. Rev. Lett.* 125(12), 126403 (2020)
211. S. A. Hassani Gangaraj, C. Valagiannopoulos, and F. Monticone, Topological scattering resonances at ultralow frequencies, *Phys. Rev. Res.* 2(2), 023180 (2020)
212. C. Z. Li, A. Q. Wang, C. Li, W. Z. Zheng, A. Brinkman, D. P. Yu, and Z. M. Liao, Reducing electronic trans port dimension to topological hinge states by increasing geometry size of Dirac semimetal Josephson junctions, *Phys. Rev. Lett.* 124(15), 156601 (2020)
213. D. Călugăru, V. Juričič, and B. Roy, Higher-order topological phases: A general principle of construction, *Phys. Rev. B* 99(4), 041301 (2019)
214. H. Hu, B. Huang, E. Zhao, and W. V. Liu, Dynamical singularities of floquet higher-order topological insulators, *Phys. Rev. Lett.* 124(5), 057001 (2020)
215. B. Huang and W. V. Liu, Floquet higher-order topological insulators with anomalous dynamical polarization, *Phys. Rev. Lett.* 124(21), 216601 (2020)
216. M. Kheirkhah, Z. Yan, Y. Nagai, and F. Marsiglio, First and second order topological superconductivity and temperature driven topological phase transitions in the extended Hubbard model with spin–orbit coupling, *Phys. Rev. Lett.* 125(1), 017001 (2020)
217. M. Kheirkhah, Y. Nagai, C. Chen, and F. Marsiglio, Majorana corner flatbands in two-dimensional second order topological superconductors, *Phys. Rev. B* 101(10), 104502 (2020)
218. A. Sarsen, and C. Valagiannopoulos, Robust polarization twist by pairs of multilayers with tilted optical axes, *Phys. Rev. B* 99(11), 115304 (2019)
219. J. Noh, W. A. Benalcazar, S. Huang, M. J. Collins, K. P. Chen, T. L. Hughes, and M. C. Rechtsman, Topological protection of photonic midgap defect modes, *Nat. Photonics* 12(7), 408 (2018)
220. Y. B. Choi, Y. Xie, C. Z. Chen, J. Park, S. B. Song, J. Yoon, B. J. Kim, T. Taniguchi, K. Watanabe, J. Kim, K. C. Fong, M. N. Ali, K. T. Law, and G. H. Lee, Evidence of higher-order topology in multilayer WTe_2 from Josephson coupling through anisotropic hinge states, *Nat. Mater.* 19(9), 974 (2020)
221. B. J. Wieder, Z. Wang, J. Cano, X. Dai, L. M. Schoop, B. Bradlyn, and B. A. Bernevig, Strong and fragile topological Dirac semimetals with higher-order Fermi arcs, *Nat. Commun.* 11(1), 627 (2020)
222. B. Xie, H. X. Wang, X. Zhang, P. Zhan, J. H. Jiang, M. Lu, and Y. Chen, Higher-order band topology, *Nat. Rev. Phys.* 3(7), 520 (2021)
223. D. A. Kealhofer, L. Galletti, T. Schumann, A. Suslov, and S. Stemmer, Topological insulator state and collapse of the quantum Hall effect in a three-dimensional Dirac semimetal heterojunction, *Phys. Rev. X* 10(1), 011050 (2020)
224. B. C. Lin, S. Wang, S. Wiedmann, J. M. Lu, W. Z. Zheng, D. Yu, and Z. M. Liao, Observation of an odd integer quantum Hall effect from topological surface states in Cd_3As_2, *Phys. Rev. Lett.* 122(3), 036602 (2019)
225. S. Wang, B. C. Lin, W. Z. Zheng, D. Yu, and Z. M. Liao, Fano interference between bulk and surface states of a Dirac semimetal Cd_3As_2 nanowire, *Phys. Rev. Lett.* 120(25), 257701 (2018)

226. S. Nishihaya, M. Uchida, Y. Nakazawa, M. Kriener, Y. Kozuka, Y. Taguchi, and M. Kawasaki, Gate-tuned quantum Hall states in Dirac semimetal, *Sci. Adv.* 4(5), eaar5668 (2018)
227. L. Galletti, T. Schumann, O. F. Shoron, M. Goyal, D. A. Kealhofer, H. Kim, and S. Stemmer, Two-dimensional Dirac fermions in thin films of Cd_3As_2, *Phys. Rev. B* 97(11), 115132 (2018)
228. T. Schumann, L. Galletti, D. A. Kealhofer, H. Kim, M. Goyal, and S. Stemmer, Observation of the quantum Hall effect in confined films of the three-dimensional Dirac semimetal Cd_3As_2, *Phys. Rev. Lett.* 120(1), 016801 (2018)
229. C. Z. Chang, J. Zhang, X. Feng, J. Shen, Z. Zhang, M. Guo, K. Li, Y. Ou, P. Wei, L. L. Wang, Z. Q. Ji, Y. Feng, S. Ji, X. Chen, J. Jia, X. Dai, Z. Fang, S. C. Zhang, K. He, Y. Wang, L. Lu, X. C. Ma, and Q. K. Xue, Experimental observation of the quantum anomalous Hall effect in a magnetic topological insulator, *Science* 340(6129), 167 (2013)
230. C. Zhang, A. Narayan, S. Lu, J. Zhang, H. Zhang, Z. Ni, X. Yuan, Y. Liu, J. H. Park, E. Zhang, W. Wang, S. Liu, L. Cheng, L. Pi, Z. Sheng, S. Sanvito, and F. Xiu, Evolution of Weyl orbit and quantum Hall effect in Dirac semimetal Cd_3As_2, *Nat. Commun.* 8(1), 1272 (2017)
231. M. Uchida, Y. Nakazawa, S. Nishihaya, K. Akiba, M. Kriener, Y. Kozuka, A. Miyake, Y. Taguchi, M. Tokunaga, N. Nagaosa, Y. Tokura, and M. Kawasaki, Quantum Hall states observed in thin films of Dirac semimetal Cd_3As_2, *Nat. Commun.* 8(1), 2274 (2017)
232. C. Zhang, Y. Zhang, X. Yuan, S. Lu, J. Zhang, A. Narayan, Y. Liu, H. Zhang, Z. Ni, R. Liu, E. S. Choi, A. Suslov, S. Sanvito, L. Pi, H. Z. Lu, A. C. Potter, and F. Xiu, Quantum Hall effect based on Weyl orbits in Cd_3As_2, *Nature* 565(7739), 331 (2019)
233. S. Nishihaya, M. Uchida, Y. Nakazawa, R. Kurihara, K. Akiba, M. Kriener, A. Miyake, Y. Taguchi, M. Tokunaga, and M. Kawasaki, Quantized surface transport in topological Dirac semimetal films, *Nat. Commun.* 10(1), 2564 (2019)
234. T. Schumann, L. Galletti, D. A. Kealhofer, H. Kim, S. Goyal, and S. Stemmer, Observation of the quantum Hall effect in confined films of the three-dimensional Dirac semimetal Cd_3As_2, *Phys. Rev. Lett.* 120(1), 016801 (2018)
235. P. J. W. Moll, N. L. Nair, T. Helm, A. C. Potter, I. Kimchi, A. Vishwanath, and J. G. Analytis, Transport evidence for Fermi arc mediated chirality transfer in the Dirac semimetal Cd_3As_2, *Nature* 535(7611), 266 (2016)
236. P. N. Argyres and E. N. Adams, Longitudinal magnetoresistance in the quantum limit, *Phys. Rev.* 104(4), 900 (1956)
237. P. A. Lee and T. V. Ramakrishnan, Disordered electronic systems, *Rev. Mod. Phys.* 57(2), 287 (1985)
238. J. Wang, H. Li, C. Chang, K. He, J. S. Lee, H. Lu, Y. Sun, X. Ma, N. Samarth, S. Shen, Q. Xue, M. Xie, and M. H. W. Chan, Anomalous anisotropic magnetoresistance in topological insulator films, *Nano Res.* 5(10), 739 (2012)
239. H. T. He, H. C. Liu, B. K. Li, X. Guo, Z. J. Xu, M. H. Xie, and J. N. Wang, Disorderinduced linear magnetoresistance in (221) topological insulator Bi_2Se_3 films, *Appl. Phys. Lett.* 103(3), 031606 (2013)
240. S. Wiedmann, A. Jost, B. Fauqué, J. van Dijk, M. J. Meijer, T. Khouri, S. Pezzini, S. Grauer, S. Schreyeck, C. Brüne, H. Buhmann, L. W. Molenkamp, and N. E. Hussey, Anisotropic and strong negative magnetoresistance in the three-dimensional topological insulator Bi_2Se_3, *Phys. Rev. B* 94(8), 081302 (2016)
241. L. X. Wang, Y. Yan, L. Zhang, Z. M. Liao, H. C. Wu, and D. P. Yu, Zeeman effect on surface electron transport in topological insulator Bi_2Se_3 nanoribbons, *Nanoscale* 7(40), 16687 (2015)
242. O. Breunig, Z. Wang, A. A. Taskin, J. Lux, A. Rosch, and Y. Ando, Gigantic negative magnetoresistance in the bulk of a disordered topological insulator, *Nat. Commun.* 8(1), 15545 (2017)
243. B. A. Assaf, T. Phuphachong, E. Kampert, V. V. Volobuev, P. S. Mandal, J. Sánchez-Barriga, O. Rader, G. Bauer, G. Springholz, L. A. de Vaulchier, and Y. Guldner, Negative longitudinal magnetoresistance from the anomalous $N = 0$ Landau level in topo logical materials, *Phys. Rev. Lett.* 119(10), 106602 (2017)
244. H. J. Kim, K. S. Kim, J. F. Wang, M. Sasaki, T. Satoh, A. Ohnishi, M. Kitaura, M. Yang, and L. Li, Dirac versus Weyl fermions in topological insulators: Adler–Bell–Jackiw anomaly in transport phenomena, *Phys. Rev. Lett.* 111(24), 246603 (2013)
245. K. S. Kim, H. J. Kim, and M. Sasaki, Boltzmann equation approach to anomalous transport in a Weyl metal, *Phys. Rev. B* 89(19), 195137 (2014)
246. Q. Li, D. E. Kharzeev, C. Zhang, Y. Huang, I. Pletikosic, A. V. Fedorov, R. D. Zhong, J. A. Schneeloch, G. D. Gu, and T. Valla, Chiral magnetic effect in $ZrTe_5$, *Nat. Phys.* 12(6), 550 (2016)
247. C. L. Zhang, S. Y. Xu, I. Belopolski, Z. Yuan, Z. Lin, B. Tong, G. Bian, N. Alidoust, C. C. Lee, S. M. Huang, T. R. Chang, G. Chang, C. H. Hsu, H. T. Jeng, M. Neupane, D. S. Sanchez, H. Zheng, J. Wang, H. Lin, C. Zhang, H. Z. Lu, S. Q. Shen, T. Neupert, M. Zahid Hasan, and S. Jia, Signatures of the Adler–Bell–Jackiw chiral anomaly in a Weyl Fermion semimetal, *Nat. Commun.* 7(1), 10735 (2016)
248. X. C. Huang, L. Zhao, Y. Long, P. Wang, D. Chen, Z. Yang, H. Liang, M. Xue, H. Weng, Z. Fang, X. Dai, and G. Chen, Observation of the chiral anomaly-induced negative magnetoresistance in 3D Weyl semimetal TaAs, *Phys. Rev. X* 5(3), 031023 (2015)
249. J. Xiong, S. K. Kushwaha, T. Liang, J. W. Krizan, M. Hirschberger, W. Wang, R. J. Cava, and N. P. Ong, Evidence for the chiral anomaly in the Dirac semimetal Na_3Bi, *Science* 350(6259), 413 (2015)
250. C. Z. Li, L. X. Wang, H. W. Liu, J. Wang, Z. M. Liao, and D. P. Yu, Giant negative magnetoresistance induced by the chiral anomaly in individual Cd_3As_2 nanowires, *Nat. Commun.* 6(1), 10137 (2015)
251. C. Zhang, E. Zhang, W. Wang, Y. Liu, Z. G. Chen, S. Lu, S. Liang, J. Cao, X. Yuan, L. Tang, Q. Li, C. Zhou, T. Gu, Y. Wu, J. Zou, and F. Xiu, Room temperature chiral charge pumping in Dirac semimet-

als, *Nat. Commun.* 8(1), 13741 (2017)
252. F. Arnold, C. Shekhar, S.-C. Wu, Yan Sun, R. D. Reis, N. Kumar, M. Naumann, M. O. Ajeesh, M. Schmidt, A. G. Grushin, J. H. Bardarson, M. Baenitz, D. Sokolov, H. Borrmann, M. Nicklas, C. Felser, E. Hassinger, and B. Yan, Negative magnetoresistance without well-defined chirality in the Weyl semimetal TaP, *Nat. Commun.* 7, 11615 (2016)
253. X. J. Yang, Y. P. Liu, Z. Wang, Y. Zheng, and Z. A. Xu, Chiral anomaly induced negative magnetoresistance in topological Weyl semimetal NbAs, arXiv: 1506.03190 (2015)
254. X. Yang, Y. Li, Z. Wang, Y. Zhen, and Z. A. Xu, Observation of negative magnetoresistance and nontrivial π Berry's phase in 3D Weyl semimetal NbAs, arXiv: 1506.02283 (2015)
255. H. Wang, C. K. Li, H. Liu, J. Yan, J. Wang, J. Liu, Z. Lin, Y. Li, Y. Wang, L. Li, D. Mandrus, X. C. Xie, J. Feng, and J. Wang, Chiral anomaly and ultrahigh mobility in crystalline $HfTe_5$, *Phys. Rev. B* 93(16), 165127 (2016)
256. S. L. Adler, Axial vector vertex in spinor electrodynamics, *Phys. Rev.* 177(5), 2426 (1969)
257. J. S. Bell and R. Jackiw, A PCAC puzzle: $\pi^0 \to \gamma\gamma$ in the σmodel, *Nuovo Cim., A* 60(1), 47 (1969)
258. H. B. Nielsen and M. Ninomiya, Absence of neutrinos on a lattice (i): Proof by homotopy theory, *Nucl. Phys. B* 185(1), 20 (1981)
259. B. Bradlyn, J. Cano, Z. Wang, M. G. Vergniory, C. Felser, R. J. Cava, and B. A. Bernevig, Beyond Dirac and Weyl fermions: Unconventional quasiparticles in conventional crystals, *Science* 353(6299), aaf5037 (2016)
260. G. Chang, B. J. Wieder, F. Schindler, D. S. Sanchez, I. Belopolski, S. M. Huang, B. Singh, D. Wu, T. R. Chang, T. Neupert, S. Y. Xu, H. Lin, and M. Z. Hasan, Topological quantum properties of chiral crystals, *Nat. Mater.* 17(11), 978 (2018)
261. P. Goswami, J. H. Pixley, and S. Das Sarma, Axial anomaly and longitudinal magnetoresistance of a generic three-dimensional metal, *Phys. Rev. B* 92(7), 075205 (2015)
262. D. N. Basov, M. M. Fogler, A. Lanzara, F. Wang, and Y. Zhang, Colloquium: Graphene spectroscopy, *Rev. Mod. Phys.* 86(3), 959 (2014)
263. M. Z. Hasan and C. L. Kane, Colloquium: Topological insulators, *Rev. Mod. Phys.* 82(4), 3045 (2010)
264. J. C. Charlier, X. Blase, and S. Roche, Electronic and transport properties of nanotubes, *Rev. Mod. Phys.* 79(2), 677 (2007)
265. K. S. Novoselov, V. I. Fal′ko, L. Colombo, P. R. Gellert, M. G. Schwab, and K. Kim, A roadmap for graphene, *Nature* 490(7419), 192 (2012)
266. T. Liang, Q. Gibson, M. N. Ali, M. H. Liu, R. J. Cava, and N. P. Ong, Ultrahigh mobility and giant magnetoresistance in the Dirac semimetal Cd_3As_2, *Nat. Mater.* 14(3), 280 (2015)
267. Z. Wang, Y. Sun, X. Q. Chen, C. Franchini, G. Xu, S. Weng, X. Dai, and Z. Fang, Dirac semimetal and topological phase transitions in A_3Bi (A = Na, K, Rb), *Phys. Rev. B* 85(19), 195320 (2012)
268. Z. K. Liu, B. Zhou, Y. Zhang, Z. J. Wang, H. M. Weng, D. Prabhakaran, S. K. Mo, Z. X. Shen, Z. Fang, X. Dai, Z. Hussain, and Y. L. Chen, Discovery of a three-dimensional topological Dirac semimetal, Na_3Bi, *Science* 343(6173), 864 (2014)
269. Z. K. Liu, J. Jiang, B. Zhou, Z. J. Wang, Y. Zhang, H. M. Weng, D. Prabhakaran, S. K. Mo, H. Peng, P. Dudin, T. Kim, M. Hoesch, Z. Fang, X. Dai, Z. X. Shen, D. L. Feng, Z. Hussain, and Y. L. Chen, A stable three-dimensional topological Dirac semimetal Cd_3As_2, *Nat. Mater.* 13(7), 677 (2014)
270. S. M. Huang, S. Y. Xu, I. Belopolski, C. C. Lee, G. Chang, B. K. Wang, N. Alidoust, G. Bian, M. Neupane, C. Zhang, S. Jia, A. Bansil, H. Lin, and M. Z. Hasan, A Weyl fermion semimetal with surface Fermi arcs in the transition metal monopnictide TaAs class, *Nat. Commun.* 6(1), 7373 (2015)
271. H. M. Weng, C. Fang, Z. Fang, B. A. Bernevig, and T. Dai, Weyl semimetal phase in noncentrosymmetric transition metal monophosphides, *Phys. Rev. X* 5(1), 011029 (2015)
272. S. Y. Xu, I. Belopolski, N. Alidoust, M. Neupane, G. Bian, C. Zhang, R. Sankar, G. Chang, Z. Yuan, C. C. Lee, S. M. Huang, H. Zheng, J. Ma, D. S. Sanchez, B. K. Wang, A. Bansil, F. Chou, P. P. Shibayev, H. Lin, S. Jia, and M. Z. Hasan, Discovery of a Weyl fermion semimetal and topological Fermi arcs, *Science* 349(6248), 613 (2015)
273. B. Q. Lv, H. M. Weng, B. B. Fu, X. P. Wang, H. Miao, J. Ma, P. Richard, X. C. Huang, L. X. Zhao, G. F. Chen, Z. Fang, X. Dai, T. Qian, and H. Ding, Experimental discovery of Weyl semimetal TaAs, *Phys. Rev. X* 5(3), 031013 (2015)
274. X. Wan, A. M. Turner, A. Vishwanath, and S. Y. Savrasov, Topological semimetal and Fermi arc surface states in the electronic structure of pyrochlore iridates, *Phys. Rev. B* 83(20), 205101 (2011)
275. K. Y. Yang, Y. M. Lu, and Y. Ran, Quantum Hall effects in a Weyl semimetal: Possible application in pyrochlore iridates, *Phys. Rev. B* 84(7), 075129 (2011)
276. A. A. Burkov and L. Balents, Weyl semimetal in a topological insulator multilayer, *Phys. Rev. Lett.* 107(12), 127205 (2011)
277. H. B. Nielsen and M. Ninomiya, The Adler–Bell–Jackiw anomaly and Weyl fermions in a crystal, *Phys. Lett. B* 130, 389 (1983)
278. D. T. Son, and B. Z. Spivak, Chiral anomaly and classical negative magnetoresistance of Weyl metals, *Phys. Rev. B* 88(10), 104412 (2013)
279. D. Shoenberg, Magnetic Oscillations in Metals, Cambridge University Press, 1984
280. S. E. Sebastian, N. Harrison, E. Palm, T. P. Murphy, C. H. Mielke, R. Liang, D. A. Bonn, W. N. Hardy, and G. G. Lonzarich, A multi-component Fermi surface in the vortex state of an underdoped high-T_c superconductor, *Nature* 454(7201), 200 (2008)
281. L. Li, J. G. Checkelsky, Y. S. Hor, C. Uher, A. F. Hebard, R. J. Cava, and N. P. Ong, Phase transitions of Dirac electrons in bismuth, *Science* 321(5888), 547 (2008)
282. Z. Zhang, W. Wei, F. Yang, Z. Zhu, M. Guo, Y. Feng,

D. Yu, M. Yao, N. Harrison, R. McDonald, Y. Zhang, D. Guan, D. Qian, J. Jia, and Y. Wang, Zeeman effect of the topological surface states revealed by quantum oscillations up to 91 Tesla, *Phys. Rev. B* 92(23), 235402 (2015)
283. N. L. Brignall, The de Haasvan–Alphen effect in n-InSb and n-InAs, *J. Phys. C* 7(23), 4266 (1974)
284. Y. Zhang, Y. W. Tan, H. L. Stormer, and P. Kim, Experimental observation of the quantum Hall effect and Berry's phase in graphene, *Nature* 438(7065), 201 (2005)
285. M. Imada, A. Fujimori, and Y. Tokura, Metal–insulator transitions, *Rev. Mod. Phys.* 70(4), 1039 (1998)
286. S. L. Sondhi, S. M. Girvin, J. P. Carini, and D. Shahar, Continuous quantum phase transitions, *Rev. Mod. Phys.* 69(1), 315 (1997)
287. S. V. Kravchenko and M. P. Sarachik, Metal–insulator transition in two-dimensional electron systems, *Rep. Prog. Phys.* 67(1), 1 (2004)
288. D. J. Newson and M. Pepper, Critical conductivity at the magnetic field-induced metal–insulator transition in n-GaAs and n-InSb, *J. Phys. C* 19(21), 3983 (1986)
289. V. J. Goldman, M. Shayegan, and H. D. Drew, Anomalous Hall effect below the magnetic field induced metal–insulator transition in narrow gap semiconductors, *Phys. Rev. Lett.* 57(8), 1056 (1986)
290. M. C. Maliepaard, M. Pepper, R. Newbury, J. E. F. Frost, D. C. Peacock, D. A. Ritchie, G. A. C. Jones, and G. Hill, Evidence of a magneticfield-induced insulator metal–insulator transition, *Phys. Rev. B* 39(2), 1430 (1989)
291. P. Dai, Y. Zhang, and M. P. Sarachik, Effect of a magnetic field on the critical conductivity exponent at the metal–insulator transition, *Phys. Rev. Lett.* 67(1), 136 (1991)
292. S. Kivelson, D. H. Lee, and S. C. Zhang, Global phase diagram in the quantum Hall effect, *Phys. Rev. B* 46(4), 2223 (1992)
293. T. Wang, K. P. Clark, G. F. Spencer, A. M. Mack, and W. P. Kirk, Magnetic field-induced metal–insulator transition in two dimensions, *Phys. Rev. Lett.* 72(5), 709 (1994)
294. Y. Tomioka, A. Asamitsu, H. Kuwahara, Y. Moritomo, and Y. Tokura, Magnetic field-induced metal-insulator phenomena in $Pr_{1-x}Ca_xMno_3$ with controlled charge ordering instability, *Phys. Rev. B* 53(4), R1689 (1996)
295. D. Popović, A. B. Fowler, and S. Washburn, Metal–insulator transition in two dimensions: Effects of dis order and magnetic field, *Phys. Rev. Lett.* 79(8), 1543 (1997)
296. X. C. Xie, X. R. Wang, and D. Z. Liu, Kosterlitz–Thouless type metal–insulator transition of a 2D electron gas in a random magnetic field, *Phys. Rev. Lett.* 80(16), 3563 (1998)
297. J. An, C. D. Gong, and H. Q. Lin, Theory of the magnetic field-induced metal–insulator transition, *Phys. Rev. B* 63(17), 174434 (2001)
298. H. Kempa, P. Esquinazi, and Y. Kopelevich, Field induced metal–insulator transition in the c axis resistivity of graphite, *Phys. Rev. B* 65(24), 241101 (2002)
299. E. V. Gorbar, V. P. Gusynin, V. A. Miransky, and I. A. Shovkovy, Magnetic field driven metal–insulator phase transition in planar systems, *Phys. Rev. B* 66(4), 045108 (2002)
300. Y. Kopelevich, J. C. M. Pantoja, R. R. da Silva, and S. Moehlecke, Universal magnetic field driven metal insulator–metal transformations in graphite and bismuth, *Phys. Rev. B* 73(16), 165128 (2006)
301. D. J. W. Geldart and D. Neilson, Quantum critical behavior in the insulating region of the two-dimensional metalinsulator transition, *Phys. Rev. B* 76(19), 193304 (2007)
302. S. Calder, V. O. Garlea, D. F. McMorrow, M. D. Lumsden, M. B. Stone, J. C. Lang, J. W. Kim, J. A. Schlueter, Y. G. Shi, K. Yamaura, Y. S. Sun, Y. Tsujimoto, and A. D. Christianson, Magnetically driven metal–insulator transition in $NaOsO_3$, *Phys. Rev. Lett.* 108(25), 257209 (2012)
303. K. Ueda, J. Fujioka, B. J. Yang, J. Shiogai, A. Tsukazaki, S. Nakamura, S. Awaji, N. Nagaosa, and Y. Tokura, Magnetic field-induced insulator–semimetal transition in a pyrochlore $Nd_2Ir_2O_7$, *Phys. Rev. Lett.* 115(5), 056402 (2015)
304. Z. Tian, Y. Kohama, T. Tomita, H. Ishizuka, T. H. Hsieh, J. J. Ishikawa, K. Kindo, L. Balents, and S. Nakatsuji, Field-induced quantum metal–insulator transition in the pyrochlore iridate $Nd_2Ir_2O_7$, *Nat. Phys.* 12(2), 134 (2016)
305. P. Wang, Y. Ren, F. Tang, P. Wang, T. Hou, H. Zeng, L. Zhang, and Z. Qiao, Approaching three-dimensional quantum Hall effect in bulk $HfTe_5$, *Phys. Rev. B* 101(16), 161201 (2020)
306. M. Vojta, Quantum phase transitions, *Rep. Prog. Phys.* 66(12), 2069 (2003)
307. H. Löhneysen, A. Rosch, M. Vojta, and P. Wölfle, Fermi-liquid instabilities at magnetic quantum phase transitions, *Rev. Mod. Phys.* 79(3), 1015 (2007)
308. E. Abrahams, P. W. Anderson, D. C. Licciardello, and T. V. Ramakrishnan, Scaling theory of localization: Absence of quantum diffusion in two dimensions, *Phys. Rev. Lett.* 42(10), 673 (1979)
309. F. J. Wegner, Electrons in disordered systems: scaling near the mobility edge, *Z. Phys. B* 25, 327 (1976)
310. W. L. McMillan, Scaling theory of the metal-insulator transition in amorphous materials, *Phys. Rev. B* 24(5), 2739 (1981)
311. C. A. Stafford and A. J. Millis, Scaling theory of the Mott–Hubbard metal–insulator transition in one dimension, *Phys. Rev. B* 48(3), 1409 (1993)
312. B. Huckestein, Scaling theory of the integer quantum Hall effect, *Rev. Mod. Phys.* 67(2), 357 (1995)
313. V. Dobrosavljević, E. Abrahams, E. Miranda, and S. Chakravarty, Scaling theory of two-dimensional metal–insulator transitions, *Phys. Rev. Lett.* 79(3), 455 (1997)
314. A. Pelissetto and E. Vicari, Critical phenomena and renormalization group theory, *Phys. Rep.* 368(6), 549 (2002)
315. G. Grüner, Density Waves in Solids, CRC Press, 2018
316. T. Giamarchi, Quantum Physics in One Dimension, Vol. 121, Clarendon Press, 2003
317. H. Watanabe and Y. Yanase, Nonlinear electric transport

in odd parity magnetic multipole systems: Application to Mn-based compounds, *Phys. Rev. Res.* 2(4), 043081 (2020)
318. S. Y. Xu, Y. Xia, L. A. Wray, S. Jia, F. Meier, J. H. Dil, J. Osterwalder, B. Slomski, A. Bansil, H. Lin, R. J. Cava, and M. Z. Hasan, Topological phase transition and texture inversion in a tunable topological insulator, *Science* 332(6029), 560 (2011)
319. Y. Gong, J. Guo, J. Li, K. Zhu, M. Liao, X. Liu, Q. Zhang, L. Gu, L. Tang, X. Feng, D. Zhang, W. Li, C. Song, L. Wang, P. Yu, X. Chen, Y. Wang, H. Yao, W. Duan, Y. Xu, S. C. Zhang, X. Ma, Q. K. Xue, and K. He, Experimental realization of an intrinsic magnetic topological insulator, *Chin. Phys. Lett.* 36(7), 076801 (2019)
320. M. M. Otrokov, I. P. Rusinov, M. Blanco-Rey, M. Hoffmann, A. Y. Vyazovskaya, S. V. Eremeev, A. Ernst, P. M. Echenique, A. Arnau, and E. V. Chulkov, Unique thickness dependent properties of the van Der Waals interlayer antiferromagnet $MnBi_2Te_4$ films, *Phys. Rev. Lett.* 122(10), 107202 (2019)
321. C. Reeg, O. Dmytruk, D. Chevallier, D. Loss, and J. Klinovaja, Zero energy Andreev bound states from quantum dots in proximitized Rashba nanowires, *Phys. Rev. B* 98(24), 245407 (2018)
322. C. A. Li, S. B. Zhang, J. Li, and B. Trauzettel, Higher-order Fabry–Pérot interferometer from topological hinge states, *Phys. Rev. Lett.* 127(2), 026803 (2021)
323. L. D. Landau, Paramagnetism of metals, *Eur. Phys. J. A* 64(9–10), 629 (1930)
324. Z. Zhu, R. McDonald, A. Shekhter, B. Ramshaw, K. A. Modic, F. Balakirev, and N. Harrison, Magnetic field tuning of an excitonic insulator between the weak and strong coupling regimes in quantum limit graphite, *Sci. Rep.* 7(1), 1733 (2017)
325. S. Galeski, X. Zhao, R. Wawrzyńczak, T. Meng, T. Förster, P. M. Lozano, S. Honnali, N. Lamba, T. Ehmcke, A. Markou, Q. Li, G. Gu, W. Zhu, J. Wosnitza, C. Felser, G. F. Chen, and J. Gooth, Unconventional Hall response in the quantum limit of $HfTe_5$, *Nat. Commun.* 11(1), 5926 (2020)
326. S. Wang, A. E. Kovalev, A. V. Suslov, and T. Siegrist, A facility for X-ray diffraction in magnetic fields up to 25 t and temperatures between 15 and 295 K, *Rev. Sci. Instrum.* 86(12), 123902 (2015)
327. Y. Narumi, K. Kindo, K. Katsumata, M. Kawauchi, C. Broennimann, U. Staub, H. Toyokawa, Y. Tanaka, K. Kikkawa, T. Yamamoto, M. Hagiwara, T. Ishikawa, and H. Kitamura, X-ray diffraction studies in pulsed high magnetic fields, *J. Phys. Conf. Ser.* 51, 494 (2006)
328. P. Pototsching, E. Gratz, H. Kirchmayr, and A. Lindbaum, X-ray diffraction in magnetic fields, *J. Alloys Compd.* 247(1–2), 234 (1997)
329. P. Wang, F. Tang, P. Wang, H. Zhu, C. W. Cho, J. Wang, X. Du, Y. Shao, and L. Zhang, Quantum transport properties of β-Bi_4I_4 near and well beyond the extreme quantum limit, *Phys. Rev. B* 103(15), 155201 (2021)